Model Prediction and Rule Based Energy Management Strategy for a Plug-in Hybrid Electric Vehicle With Hybrid Energy Storage System

Shiyao Zhou, Ziqiang Chen, *Senior Member, IEEE*, Deyang Huang, and Tiantian Lin

***Abstract*—This article presents an energy management strategy (EMS) design and optimization approach for a plug-in hybrid electric vehicle (PHEV) with a hybrid energy storage system (HESS) which contains a Li–Ti–O battery pack and a Ni–Co–Mn battery pack. The EMS shares power flows within the hybrid powertrain, and it employs a dual fuzzy logical controller whose inputs are predictions for PHEV powertrain states. An elitist nondominant genetic algorithm using a model in loop simulation approach as fitness functions is implemented to multiobjective optimization for the EMS under worldwide light-duty test cycles. The optimal objectives are improving PHEV mileage, minimizing battery packs capacity fades, reducing HESS degradation inconsistency, and minimizing driving cost unit distance. A hardware in loop test bench has been established to verify EMS performances in embedded systems. The test results under new European driving cycles demonstrate that optimized EMSs remain appropriate for different driving cycles and their performances are close to dynamic programming based offline optimal solutions. Due to the contributions of both the HESS and the optimized EMS, the PHEV energy efficiency has been improved by 1.6%–2.5% and the PHEV energy storage system cycle life can be improved by 159%–203%.**

***Index Terms*—Energy management strategy (EMS), hybrid energy storage system (HESS), multiobjective optimization, plug-in hybrid electric vehicle (PHEV).**

NOMENCLATURE

Abbreviations

APU	Assistant power unit.
BSFC	Brake specific fuel consumption.
CD	Charge-Depleting.
CS	Charge-Sustaining.
DAEKF	Dual adaptive extended Kalman filter.
DFLC	Dual fuzzy logical controller.
EMS	Energy management strategy.
HIL	Hardware in loop.
LTO	Li–Ti–O battery.
HESS	Hybrid energy storage system.
MF	Membership function.
MG	Motor/generator.
MIL	Model in loop.
NCM	Ni–Co–Mn battery.
NEDC	New European Driving Cycle.
NSGA-II	Elitist nondominant genetic algorithm.
OCV	Open-circuit voltage.
PHEV	Plug-in hybrid electric vehicle.
SoC	State of charge.
SoP	State of power capability.
WLTC	Worldwide Light-duty Test Cycle.

Superscript

chg	At the state of charge.
dis	At the state of discharge.
i	*i*th in-pack unselected cell.
s	Selected cell.

Subscript

n	*n*th sampling time step.

Manuscript received April 8, 2020; revised August 28, 2020; accepted September 27, 2020. Date of publication October 1, 2020; date of current version January 22, 2021. This work was supported by the National Natural Science Foundation of China under Grant 51677119. The paper was presented in part at the 2019 IEEE 3th International Electrical and Energy Conference and awarded best paper, Beijing, China, Sep. 7–9, 2019. Recommended for publication for Associate Editor T. Dragicevic. *(Corresponding author: Ziqiang Chen.)*

Shiyao Zhou, Deyang Huang, and Tiantian Lin are with the State Key Laboratory of Ocean Engineering, Shanghai Jiao Tong University, Shanghai 200240, China (e-mail: shiyaozhou_sjtu@outlook.com; 1021226087@sjtu.edu.cn; ttlinet@sjtu.edu.cn).

Ziqiang Chen is with the State Key Laboratory of Ocean Engineering, Shanghai Jiao Tong University, Shanghai 200240, China, and also with the Collaborative Innovation Center for Advanced Ship and Deep-Sea Exploration, Shanghai Jiao Tong University, Shanghai 200240, China (e-mail: chenziqiang@sjtu.edu.cn).

Color versions of one or more of the figures in this article are available online at https://ieeexplore.ieee.org.

Digital Object Identifier 10.1109/TPEL.2020.3028154

I. INTRODUCTION

DUE to the shortage of fossil energy and challenges of air pollution, plug-in hybrid electric vehicles (PHEVs) have been developed for applications in automobile industry to acquire better energy economy and lower exhaust emissions [1]–[3]. As one of the major components of a PHEV, battery performance determines the safety, reliability, and efficiency of vehicular power system [4], [5]. The vehicle instantaneous acceleration and maximum speed performance are affected by battery pack power capability [6], [7]. However, high and surge power shocks would accelerate the battery degradation [8]–[10]. Thus, the contradiction between vehicle dynamic performance and battery capacity fading impedes the further development and penetration of PHEVs [11]. To solve this problem, hybrid energy storage systems (HESSs), which combine ultra-capacitors (UCs) and electrochemical batteries, have been widely studied in recent years [12]–[16]. Batteries with the features of high energy

density and UCs with the features of both high power density and long cycle life can complement with each other, resulting in reducing the high peak power impact on batteries and recovering more regenerative kinetic energy [17]. Therefore, the life span of batteries can be prolonged and the energy economy can be improved within the whole vehicle life cycle [18]–[20].

Nevertheless, UCs have defects of low energy density, low cell voltage, and high price [21]. Given the strict weight and volume limitation to vehicular equipment, battery and UC composed HESSs are more commonly applied to buses or trucks [22] rather than passenger vehicles in practice. Fortunately, with the development of Li-ion battery, the Li–Ti–O battery (LTO) with merits of the high power density and the long cycle life is more suitable for passenger vehicles than UCs due to its higher cell voltage and larger energy density [23]. In this article, a Ni–Co–Mn battery (NCM) pack and a LTO pack are employed to compose the HESS of target PHEV.

To effectively exert the potential of HESS, the HESS topology should be comprehensively considered [24]. The semiactive HESS, which only employs one dc/dc converter, offers a better balance between performance and capital cost in comparison with the active and passive HESS [25]. In this article, a semiactive HESS is adopted in which a bidirectional dc/dc converter decouples the NCM pack from the dc bus.

The PHEV energy economy and battery packs' cycle life highly depend on the power distribution between the assistant power unit (APU) and battery packs. Thus, the energy management strategy (EMS) should be seriously designed. In recent years, researchers have widely dedicated to explore the EMSs for hybrid vehicles and HESSs, which can be mainly categorized as online and offline strategies [26]. The online EMS can be implemented in real-time systems, including rule-based control strategies, model predictive control strategies, heuristic algorithms, etc. The most widely applied strategy is the rule-based control strategy [27]. In [28], a fuzzy logic based EMS for parallel hybrid vehicles is employed to distribute the power flows of the motor/generator (MG) and the combustion engine to improve the vehicles fuel economy. In [29], a flatness control technique and a fuzzy logic based EMS are applied to a HESS, which consists of fuel cells, batteries, and UCs. The study shows that the EMS is suitable for different hybrid operating modes. A three-mode rule-based strategy for a battery/UC composed HESS is evaluated in [30] and simulation results show that the EMS can maximize HESS capacity and minimize the energy consumption of the HESS. Although the mentioned references have verified that rule-based EMSs have highly stabile and intelligent real-time performance, their validity highly depends on designers' experience. To further improve the performance of electric vehicles with HESS, model predictive control strategies have been developed in [31]–[33]. Model predictive control strategies with the object of minimize cost function for battery and UC composed HESSs are proposed in [31] and [32] whose prediction models are used to estimate the future HESS states according to the vehicle required power. Song *et al.* [31] used a linearized system model directly to estimate the battery module current and UC module terminal voltage, which are variables of the cost function. Hredzak *et al.* [32] established a HESS state-space model and a Kalman state estimator is used to predict HESS states. In Hredzak *et al.* [33], the future vehicle speed is predicted by a torque requirement exponentially decreasing model and the predicted vehicle speed is used by the EMS to destine output powers of the APU, the battery pack, and the UC pack. However, in practical applications, the action of the driver is random and the prediction models are hard to ensure the impersonality of the future vehicle speed or vehicle required power prediction in a long prediction interval scale.

The optimize-based offline strategies, such as Pontryagin's minimum principle algorithm (PMP), genetic algorithm (GA), dynamic programming (DP), and neural network, can achieve a globally optimal performance [33]. However, it is not viable for employing these optimization methods in real-time systems due to their defects of long computational time and high memory resources requirement [34]. Given the generalization of vehicular networking technologies, offline optimization methods are feasible to be applied in cloud computing centers, in which the vehicle historical information and drivers' driving habits are stored. The EMSs optimized in computing centers can be wirelessly bootloaded to onboard electronic controllers through the over-the-air technology. PMP and DP approaches are commonly used as offline optimum solutions to verify the performance of other EMSs because of their large computational cost and complex calculation processes, and GA is more suitable for tuning parameters of online EMSs. Vinot and Trigui [35] presented a rule-based parameterized EMS for a HEV and compares the EMS with the optimal strategy given by PMP approach. Then, research works optimized the rule-based EMS by traversing method and real car tests show that the battery rms current is reduced by 15% at the cost of 2%–3% higher fuel consumption. In [17], a fuzzy logic based EMS for an electric bus with a battery/UC composed HESS is optimized by GA taking the total energy consumption and the cycle life of battery into account. The performance of the optimized EMS is close to the DP-based optimal strategy. Nevertheless, Yu *et al.* [17] lack mathematical models to evaluate the battery cycle life extension quantifiably. Furthermore, the fitness function in [17] is a linear combination of objective functions, which is a pseudomultiobjective optimization.

Most of the references mentioned above focused on the EMS for the vehicles with two power sources (multiple-input single-output system, MISO) and few of them studied on the power flow control between three or more power sources (multiple-input multiple-output system, MIMO). We propose an innovative EMS, in which a dual fuzzy logical controller (DFLC) is integrated with a HESS state prediction module and a PHEV required power prediction module. The output powers of the APU and two packs are determined by the EMS. A novel multiobjective optimization method based on elitist nondominant GA (NSGA-II), in which model in loop (MIL) simulation results are employed as fitness functions, is adopted to tune the membership functions (MFs) of the integrated strategy. In MIL simulation process, quantifiable evaluation models are used to calculate the fitness functions of optimal objects, including the PHEV energy efficiency, battery pack capacity fades, and degradation inconsistency between two packs in HESS. An innovative hardware

TABLE I
ARCHETYPAL NCM PACK PARAMETERS

Parameters	Value
Battery cell positive material	NCM523
Battery cell nominal capacity	30Ah
Battery cell energy density	195w·h/kg
Battery cell rated current range(10s)	-90A ~ 150A
Battery cell operating current range	-45A ~ 90A
Battery cell operating voltage range	3.00V ~ 4.20V
Number of battery cells in parallel	2
Number of battery cells in series	96
Battery pack energy capacity	21.3kw·h
SoC usage window	15% ~ 95%

in loop (HIL) test bench is adopted to verify whether optimized EMSs remain relevant for different driving cycles.

The rest of this article is organized as follows. Section II illustrates the problem faced by the target PHEV and modeling of PHEV power system. In Section III, an integrated model prediction and a rule-based EMS is developed. After that, a NSGA-II optimization approach for the EMS based on MIL approach is proposed in Section IV. Section V details the verification and discussion of the optimized EMS. Finally, Section VI concludes this article.

II. System Modeling

A. Problem Description

The parameters of the PHEV archetypal battery pack are given in Table I. The rated current range of the archetypal battery pack is −120 to 300 A (negative for charge, positive for discharge). In order to extended cycle life of the battery pack, the operating current range of battery pack is limited to −90 to 180 A, and the cell operating voltage range is restricted to 3.00–4.20 V, resulting in a limitation to battery pack state of power capability (SoP). SoP is the ability of a battery to accept or deliver power at a given time [36], and the limitation of the battery pack SoP would cause the PHEV energy efficiency decrease, as shown in Fig. 1, along with the vehicle speed profile and covered distance of new European driving cycle (NEDC). Fig. 1(b) and (c) shows the PHEV MGs' power flows and energy flows during the NEDC revolving drum test with different current range restrictions. In comparison with Fig. 1(c), more recovery energy is absorbed by the battery pack in Fig. 1(b) at the cost of shorter pack life span.

Therefore, a HESS is carried out to improve the target PHEV energy efficiency and prolong the battery pack life span. The archetypal battery pack contains two paralleled 30 Ah NCM battery modules. In considering the strict weight limitation to vehicle equipment and reducing the target PHEV chassis secondary development cost, one of the paralleled NCM module is directly replaced by a 30 Ah LTO module. Target cells adopted in this article are shown in Fig. 2 and parameters of the LTO pack are given in Table II. The battery pack state-of-charge (SoC) usage window is 15%–95%. Although adopting a HESS can recover more braking energy, the electric energy conversion loss in a HESS is larger than in the archetypal NCM pack. If we equip the target PHEV with a HESS matched up with an inappropriate EMS, the PHEV mileage may be inferior to using a single pack.

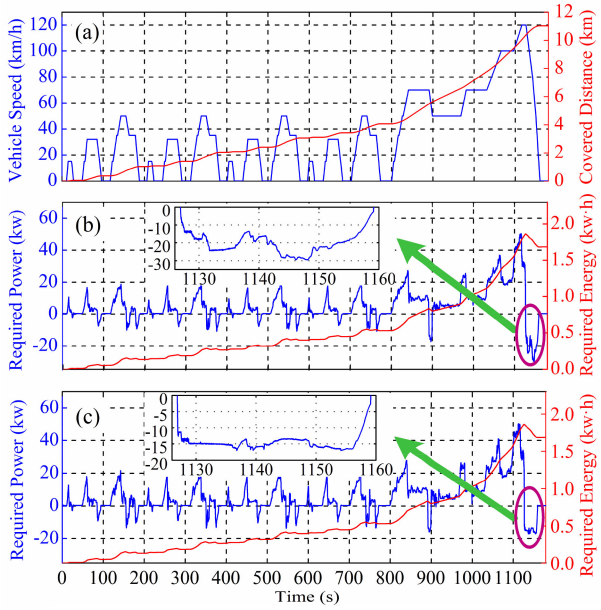

Fig. 1. Target PHEV revolving drum test results under NEDC. (a) Speed profile and covered distance. (b) MGs power and energy requirement without current restriction. (c) MGs power and energy requirement within the operating current range.

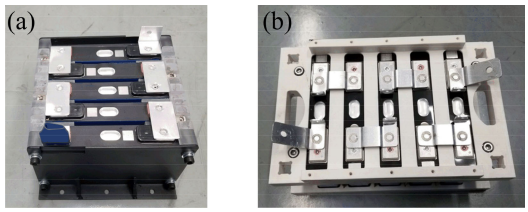

Fig. 2. Cells used in HESS. (a) NCM cells. (b) LTO cells.

TABLE II
LTO PACK PARAMETERS

Parameters	Value
Battery cathode material	$Li_4Ti_5O_{12}$
Battery cell nominal capacity	30Ah
Battery cell energy density	105w·h/kg
Battery cell operating voltage range	1.80V ~ 2.80V
Battery cell rated current range(10s)	-240A ~ 300A
Battery cell operating current range	-150A ~ 240A
Battery pack energy capacity	6.8kw·h
SoC usage window	15% ~ 95%

B. PHEV Power System Configuration

Predicting the dynamic power requirement of the target PHEV is essential to an EMS. Most research works on EV/HEV with HESS ignore the driveline efficiency, MG torque characteristics, torque distribution between front and rear wheel when calculating the PHEV power requirement. To compensate for this, a simplified PHEV hybrid system model has been constructed in Fig. 3 to evaluate the PHEV required power. The APU contains a 1.5 L gasoline engine and an integrated starter generator (ISG). The power flow of the NCM pack is controlled actively by a buck/boost bidirectional dc/dc converter and the LTO pack output power is controlled passively.

The target PHEV is equipped with two MGs, which are powered by the HESS and the APU. The reduction gear ratio

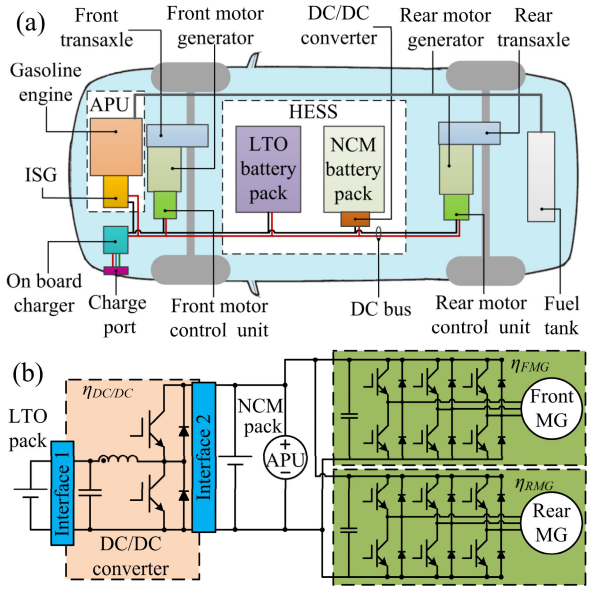

Fig. 3. Hybrid power system schematic. (a) PHEV powertrain configuration. (b) High-voltage system schematic.

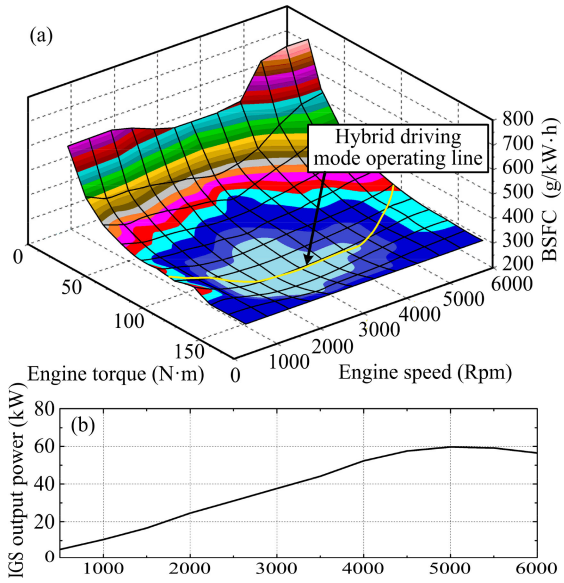

Fig. 4. APU fuel consumption characteristics. (a) Engine BSFC map. (b) IGS output power curve along the operating line.

between MGs and front and rear wheels are the same. The rated power of the front and rear MGs are 50 and 65 kW separately. A simplified PHEV dynamical model [36] has been proposed for describing the MGs overall torque as follows:

$$\begin{aligned} T_{\mathrm{MG-total}} &= T_{\mathrm{RMG}} + T_{\mathrm{FMG}} \\ &= \frac{r_w i_t}{\eta_T}\left[-mgf\cos\alpha + mg\sin\alpha + \frac{C_D A}{21.15}u_a \right. \\ &\quad \left. + \frac{du_a}{dt}\left(m + \frac{J_w}{2\pi} + \frac{J_{\mathrm{FMG}} + J_{\mathrm{RMG}}}{2\pi i_t}\right)\right] \end{aligned} \tag{1}$$

where T_{RMG} is the abbreviation of the rear MG torque, T_{FMG} is the front MG torque, r_w is the wheel radius, i_t is the transmission reduction ratio, $\eta_T = 1/\eta_t$ in propulsion process, $\eta_T = \eta_t$ in braking process (η_t is a constant transmission efficiency), m is the PHEV mass, f denotes the friction coefficient, α denotes the road gradient, J_w denotes the equivalent rotational inertia of the wheel and transaxle, J_{RMG} and J_{FMG} are rotational inertias of MGs, C_D is PHEV drag coefficient, A is PHEV windward area, g is gravitational acceleration, and u_a is the vehicle speed. The MGs' torque distribution follows ideal propulsion/braking torque distribute strategy [37]

$$\begin{aligned} T_{\mathrm{FMG}} = \frac{1}{2}\left(\frac{mgi_t}{h_g\eta_T r_w}\sqrt{L_R^2 + \frac{4T_{\mathrm{RMG}}h_g(L_F+L_R)\eta_T r_w}{mgi_t}}\right. \\ \left. - \frac{mgi_t}{h_g\eta_T r_w} - 2T_{\mathrm{RMG}}\right) \end{aligned} \tag{2}$$

$$\begin{aligned} T_{\mathrm{RMG}} = \frac{1}{2}\left(\frac{mgi_t}{h_g\eta_T r_w}\sqrt{L_F^2 + \frac{4T_{\mathrm{FMG}}h_g(L_F+L_R)\eta_T r_w}{mgi_t}}\right. \\ \left. - \frac{mgi_t}{h_g\eta_T r_w} - 2T_{\mathrm{FMG}}\right) \end{aligned} \tag{3}$$

where L_F and L_R are horizontal distances between the vehicle gravity center and two wheel axles, respectively, h_g is the height of the vehicle gravity center, (2) is the torque distribution equation in propulsion process, and (3) is the torque distribution equation in braking process. The calculated T_{RMG} and T_{FMG} should satisfy the MGs performance curves constraint. All parameters in (1)–(3) are calibrated by the revolving drum test results in Fig. 1(b). The MG overall efficiencies η_{FMG} and η_{RMG} are functions of u_a and MGs' torque. Thus, η_{RMG} and η_{FMG} can be located in MG efficiency map. Then, PHEV required power can be solved by the following:

$$P_{\mathrm{Req}} = \frac{u_a}{r_w i_t}\left(\frac{T_{\mathrm{RMG}}}{\eta_{\mathrm{RMG}}} + \frac{T_{\mathrm{FMG}}}{\eta_{\mathrm{FMG}}}\right). \tag{4}$$

C. APU Fuel Consumption Model

An engine brake specific fuel consumption (BSFC) model as presented in Fig. 4(a) is essential for quantifiably evaluating the PHEV fuel consumption. The operating line for hybrid mode represents the engine optimal torque at different engine rotational speeds. The design of the hybrid driving mode operating line comprehensively considered the fuel consumption, the engine torque performance at low speed and ISG torque constraints at high speeds. Fig. 4(b) shows the ISG output power at different rotational speeds. If the engine rotational speed is higher than 5000 r/min, the APU performance will be deteriorating. Therefore, the engine rotational speed is limited to 500–5000 r/min.

When the APU output power is stabilized, the instantaneous fuel consumption can be settled along the operating line. If the APU output power is dynamically varying, instantaneous engine torque estimation should take both the equivalent rotational inertia J_{APU} and the angular acceleration $d\omega_{\mathrm{APU}}/dt$ of the APU

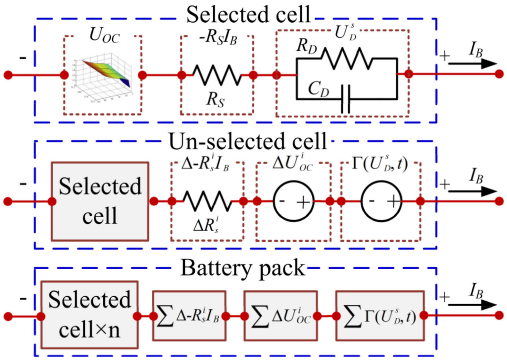

Fig. 5. Schematic of inconsistent model for battery pack.

into consideration

$$T_{\mathrm{Eng}} = T_{\mathrm{OL}} + J_{\mathrm{APU}} d\omega_{\mathrm{APU}}/dt \tag{5}$$

where T_{Eng} is the engine torque, and T_{OL} denotes the torque value settled on the operating line according to current engine speed. Utilizing T_{Eng} and ω_{APU}, the instantaneous APU fuel consumption can be located on BSFC map. In addition, it is assumed that the engine has been warmed up. The measured that once APU start-up fuel consumption is 1.24 g and the electric energy consumption is about 1.1 W·h.

D. HESS Thermal, Electrical, and Degradation Models

In general, a series connected battery system exists parameter inconsistencies between cells. Thus, it is essential to estimate every cell states in-pack for ensuring the efficient and safe operation. Fig. 5 presents the schematic of inconsistent model for battery pack [38], which can be divided into three steps: 1) modeling for the selected cell in-pack; 2) modeling for unselected cells in-pack; and 3) modeling for the battery pack. The equivalent circuit model for the selected cell is one-state Thevenin model. The series resistance (R_S) denotes the electrical resistance of cell components and contact resistance between battery cells. The diffusion resistance (R_{D}) and the diffusion capacitance (C_D) describe the diffusion voltage (U_D) characteristic. The open circuit voltage (OCV, U_{OC}) is a power source of the model related with SoC and cell average temperature. Thus, a 3-D response surface model is proposed

$$U_{\mathrm{OC}}(z, T_P) = \kappa_0 + \kappa_1 z + \kappa_2 z^2 + \kappa_3 z^3 + \kappa_4/z + \kappa_5 \mathrm{In}(z) + \kappa_6 \mathrm{In}(1-z) \tag{6}$$

where z represents battery cell SoC, T_P denotes the battery pack average temperature, and κ_i ($i = 0, 1, \ldots, 6$) depicts the temperature depended analytic functions. Given battery cell maximum available capacity varying with temperature, aging state, and current load, we use the battery cell nominal capacity in SoC definition [39]. Therefore, the battery cell SoC is the ratio of the remaining capacity to the nominal capacity C_N of a cell, and the relation between SoC and cell current flowing is formulated as follows:

$$z(t) = z(t_0) - \int_{t_0}^{t} \frac{\eta_B}{C_N} I_B(\tau) d\tau \tag{7}$$

TABLE III
BATTERY CHARGE COULOMB EFFICIENCY

Current rate	0.5	1	2	4	8
η_{NCM}	0.999	0.998	0.994	--	--
η_{LTO}	0.999	0.998	0.996	0.988	0.961

TABLE IV
DC/DC CONVERTER EFFICIENCY MAP

I_{DC} \ P_{DC}	±5kW	±10kW	±15kW	±20kW	+35kW
±10A	94%	96%	97%	--	--
±30A	92%	96%	96%	95%	90%
±50A	89%	95%	95%	93%	88%
+90A	--	92%	93%	92%	84%

where I_B is the battery cell current and η_B is the cell coulomb efficiency ($\eta_B = 1$ for discharge). Charge coulomb efficiencies of NCM and LTO cells are conducted in Table III.

The dynamic process of the selected cell terminal voltage can be expressed as follows:

$$\begin{cases} \dot{U}_D^s = -\frac{1}{R_D C_D} U_D^s + \frac{1}{C_D} I_B \\ U_T^s = U_{OC}^s - U_D^s - R_S I_B. \end{cases} \tag{8}$$

In terms of modeling for unselected cells in-pack, considering the inconsistency between the selected cell and unselected cells, a bias correction model is proposed

$$U_T^i = U_{\mathrm{OC}}^s + \Delta U_{\mathrm{OC}}^i + \Gamma_i(U_D^s, t) - I_B(R_S^s + \Delta R_S^i). \tag{9}$$

The model for unselected cell i contains four parts: selected cell model, ohmic resistance bias correction factor ΔR_S^i, OCV bias correction factor, and diffusion voltage similarity function $\Gamma_i(U_D^s, t)$, which is a time-varying function calculated by the following equation:

$$\Gamma_i(U_{D,t}^s, t) = [\beta_{2,t_0}^i (t-t_0)^2 + \beta_{1,t_0}^i (t-t_0) + \beta_{0,t_0}^i] U_{D,t}^s \tag{10}$$

where β_0 , β_1 , and β_2 are correction factors, t represents current sampling time, and t_0 denotes the moment of the last inconsistencies estimation for unselected cell i. Then, the voltage of series-connected battery pack can be calculated with the sum of the selected cell and unselected cells terminal voltages.

$$U_{T,t}^P = n U_{T,t}^s + \sum_{i=0}^{n-1} \left(\Delta U_{OC,t_0}^i - \Delta R_{s,t_0}^i I_{B,t} + \Gamma_i(U_{D,t}^s, t) \right). \tag{11}$$

The power load on NCM pack is decoupled from dc bus by a dc/dc converter. Therefore, a quantifiable dc/dc converter efficiency model is essential to PHEV powertrain modeling. Normally, a response surface $\eta_{\mathrm{DC}}(I_{\mathrm{DC}}, P_{\mathrm{DC}})$-based efficiency map shown in Table IV is employed to describe the converter efficiency [33], in which P_{DC} and I_{DC} are the dc/dc converter power flow and current flow toward the dc bus, respectively. If the terminal voltages of two battery packs and P_{DC} are known, the NCM pack current I_B^{NCM} toward the converter can be computed

TABLE V
DEGRADATION MODEL PARAMETERS

Battery type	C_0	C_1	E_a	ϑ
NCM	0.0055	-1221	18985	0.891
LTO	0.0014	-1052	19744	0.815

by the following:

$$I_B^{\mathrm{NCM}} = \begin{cases} \dfrac{P_{\mathrm{DC}}\eta_{\mathrm{DC}}\left(P_{\mathrm{DC}}/U_T^{P,\mathrm{LTO}},P_{\mathrm{DC}}\right)}{U_T^{P,\mathrm{NCM}}} & P_{\mathrm{DC}}<0 \\ \dfrac{P_{\mathrm{DC}}}{\eta_{\mathrm{DC}}\left(P_{\mathrm{DC}}/U_T^{P,\mathrm{LTO}},P_{\mathrm{DC}}\right)U_T^{P,\mathrm{NCM}}} & P_{\mathrm{DC}}\geq 0. \end{cases} \tag{12}$$

A battery degradation model is important to evaluate battery pack capacity fades with different EMSs. However, the degradation of the battery is influenced by temperatures, depths of discharge, and current loads. Therefore, a semiempirical battery degradation model proposed in [24], which contains all these factors, is adopted in this article. The discrete formula of the pack degradation model can be described as follows:

$$Q_{\mathrm{Loss},n+1} = \frac{|\eta I_{B,n}|\,\Delta t}{3600} C_0^{\frac{1}{\vartheta}}\vartheta e^{-\frac{E_a C_N + C_1|\eta_{B,n}I_{B,n}|}{\vartheta R T_P C_N}} Q_{\mathrm{Loss},n}^{\frac{\vartheta-1}{\vartheta}} + Q_{\mathrm{Loss},n} \tag{13}$$

where $Q_{\mathrm{Loss},n}$ and $Q_{\mathrm{Loss},n+1}$ are, respectively, the accumulated battery capacity loss percentages at sampling time of t_n and t_{n+1}, Δt is the sampling period, C_0 is the pre-exponential factor, E_a is the activation energy, R is the gas constant, C_0 is the compensation factor of $|I_B|$, A_h is the battery total amp-hour throughput, ϑ is a time factor, and T_P is the average temperature of the battery pack. The degradation model parameters of adopted cells provided by the manufacturer are shown in Table V.

The battery thermal model is necessary for battery pack capacity fades evaluation and SoP estimator with thermal constraints. It is assumed that the temperature field in the battery pack is equally distributed due to a well-designed pack heat emission structure. Then, the Bernardi model, which is composed of reversible heat, polarization heat, and ohmic heat, is used as the cell thermal output model [40]

$$Q_T = \left(U_{\mathrm{OC}} - U_T - T_P\frac{\delta U_{\mathrm{OC}}}{\delta T_P}\right) I_B \tag{14}$$

where T_P is the pack average temperature, $\delta U_{\mathrm{OC}}/\delta T_P$ is the OCV gradient with T_P. The main thermal loss of a battery pack is the air forced convection heat transfer, so the thermal balance equation of the battery pack can be formulated as

$$\begin{cases} Q_T^P = \sum_{i=0}^{k-1} Q_T^i = (U_{\mathrm{OC},n}^P - U_{T,t}^P - T_P\frac{\delta U_{\mathrm{OC},n}^P}{\delta T_P})I_B \\ \dot{T}_P = \frac{1}{m_P C_P}\left[Q_T^P - h_P A_P(T_P - T_{\mathrm{Air}})\right] \end{cases} \tag{15}$$

where m_P is the battery pack mass, C_P is the specific heat capacity of the battery pack, h_P is the heat exchange coefficient, A_P is the heat exchange area, T_{Air} is the cooling air temperature, and k is the in-pack cell number. Then, we can get the discrete formula of the thermal model

$$T_{P,n+1} = e^{-\frac{\Delta t a_1}{a_2}} T_{P,n} + \left(1 - e^{-\frac{\Delta t a_1}{a_2}}\right) \times \frac{(U_{\mathrm{OC},n}^P - U_{T,t}^P)I_{B,n} + h_P A_P T_{\mathrm{Air}}}{a_2} \tag{16}$$

where $U_{\mathrm{OC},n}^P = kU_{\mathrm{OC},n}^s + \sum_{i=0}^{k-1}\Delta U_{\mathrm{OC},n}^i$, $a_1 = I_{B,n}\tau + h_P A_P$, $a_2 = m_P C_P$, and $\tau = \delta U_{\mathrm{OC}}^P(z,T)/\delta T|_{T=T_{P,n}}$.

III. EMS FOR PHEV

To guarantee the effectiveness of the EMS for the target PHEV, accurate SoC and SoP estimate approaches are proposed to predict the HESS system states. Then, DFLC is designed to divide the power flows between the APU, the dc/dc converter and the LTO pack.

A. Series Connected Battery Pack SoC Estimation

The Kalman filter is one of the commonly used algorithm for battery cell system states online estimation or perform real-time system parameters identification [41], [42]. In this article, a dual adaptive extended Kalman-filter (DAEKF) and sliding least square combined method is proposed for multitimescale SoC estimation of an inconsistent battery pack. The steps of the selected cell SoC estimation approach based on DAEKF are summarized in Table VI.

In considering that the true parameters and the SoC of Li-ion batteries change very slowly, the computing time scale ($\psi \times \Delta t$) for unselected cells in-pack is longer than the selected cell. To estimate the SoC of the *i*th unselected cell, we first rewrite the (9) into the form

$$\upsilon_{n+\psi}^i = \varphi_{n+\psi}^i \boldsymbol{\vartheta}_{n+\psi}^i \tag{17}$$

where $\boldsymbol{\vartheta}_{n+\psi}^i$ is the parameter vector estimated at sampling time of $t_{n+\psi}$ and $\boldsymbol{\vartheta}^i = [\beta_0^i, \beta_1^i, \beta_2^i, \Delta U_{OC}^i, \Delta R_S^i]^{\mathrm{T}}$, $\upsilon_{n+\psi}^i = [U_{T,n}^i, U_{T,n+1}^i \ \cdots \ U_{T,n+\psi}^i]^{\mathrm{T}}$ is the measured voltage sequence, $\varphi_{n+\psi}^i = [\gamma_n^i, \gamma_{n+1}^i \ \cdots \ \gamma_{n+\psi}^i]^{\mathrm{T}}$ is the state sequence between sampling time of t_n, and $t_{n+\psi}$, in which

$$\gamma_{n+N}^i = [U_{D,n+N}^s, U_{D,n+N}^s(N-n)\Delta t, U_{D,n+n}^s(N-n)^2\Delta t^2, 1, -I_{B,n+N}].$$

Then, we can acquire the unbiased estimation results of $\hat{\boldsymbol{\vartheta}}_{n+\psi}^i$ by using the sliding least square method

$$\hat{\boldsymbol{\vartheta}}_{n+\psi}^i = (\varphi_{n+\psi^i}^{\mathrm{T}}\varphi_{n+\psi}^i)^{-1}\varphi_{n+\psi^i}^{\mathrm{T}}\upsilon_{n+\psi}^i. \tag{18}$$

The OCV of the unselected cell *i* at sampling time t_{n+N} ($\psi \leq N < 2\psi$) is $U_{\mathrm{OC}}(z_{n+N}^s) + \Delta\hat{U}_{\mathrm{OC},n+\psi}^i$. Thus, the z_{n+N}^s of cell *i* can be determined by the OCV response surface model. After the SoCs of all cells in-pack are known, the battery pack SoC can be calculated by the following:

$$\begin{cases} z_{\mathrm{chg},n}^P = \max\left(z_n^0, z_n^1 \ \cdots \ z_n^{95}\right) & I_{B,n}<0 \\ z_{\mathrm{dis},n}^P = \min\left(z_n^0, z_n^1 \ \cdots \ z_n^{95}\right) & I_{B,n}\geq 0. \end{cases} \tag{19}$$

B. Series Connected Battery Pack SoP Estimation

The SoP computing time scale is and the prediction interval scale is $q \times \Delta t$. To find the peak discharge current or charge current of the battery pack with voltage and thermal constraints, we should solve qth degree equations. First, we suppose that the battery pack minimum charge current and the maximum discharge current are constant within the following $q \times \Delta t$

TABLE VI
PROCESS OF THE SELECTED-CELL SOC ESTIMATION

Discrete time state-space model [a]

$\theta = [R_S, R_D, C_D]^{\mathrm{T}}$, $x = [U_D^s, z^s]^{\mathrm{T}}$

$A_n = \begin{bmatrix} e^{-\frac{\Delta t}{R_{D,n}C_{D,n}}} & 0 \\ 0 & 1 \end{bmatrix}$, $B_n = \begin{bmatrix} R_{D,n}(1-e^{-\frac{\Delta t}{R_{D,n}C_{D,n}}}) \\ -\Delta t \eta_{B,n} / C_N \end{bmatrix}$, $\theta_n = \theta_{n-1}$

$x_n = A_{n-1}x_{n-1} + B_{n-1}I_{B,n-1}$, $U_{T,n}^s = U_{OC}(z_n^s) - U_{D,n}^s - R_{S,n}I_{B,n}$

Based on state-space model, we define [b]**:**

$\theta_n = \theta_{n-1} + \nu_{n-1}$, $x_n = f(x_{n-1}, \theta_{n-1}, I_{B,n-1}) + r_{n-1}$, $U_{T,n}^s = g(x_n, \theta_n, I_{B,n}) + \omega_n$,

$C_n = [1 \quad 1 \quad 1]$, $H_n = \left[0 \quad \left. \frac{\delta U_{OC}(z, T_p)}{\delta z} \right|_{z=\hat{z}_n^-} \right]$

Step 1 Initialization

For n=0, set $\hat{\theta}_0^+ = \mathrm{E}[\theta_0]$, $J_0^+ = \mathrm{E}[(\theta_0 - \hat{\theta}_0^+)(\theta_0 - \hat{\theta}_0^+)^{\mathrm{T}}]$, $\hat{x}_0^+ = \mathrm{E}[x_0]$,

$P_0^+ = \mathrm{E}[(x_0 - \hat{x}_0^+)(x_0 - \hat{x}_0^+)^{\mathrm{T}}]$

Step 2 Prior estimation time update. For n = 1, 2 ,……, compute

State estimation time update: $\hat{x}_n^- = f(\hat{x}_{n-1}^+, \hat{\theta}_{n-1}^-, I_{B,n})$

State error covariance time update [c]: $P_n^- = A_n P_{n-1}^+ A_n^{\mathrm{T}} + Q_{n-1}$

Parameter estimation time update: $\hat{\theta}_n^- = \hat{\theta}_{n-1}^-$

Parameter error covariance time update: $J_n^- = J_{n-1}^+ + V_{n-1}$

Step 3 State posteriori estimation time update

Error innovation: $e_n^- = y_n - g(\hat{x}_n^-, \hat{\theta}_n^-, I_{B,n})$

State Kalman gain matrix: $K_n = P_n^-(H_n)^{\mathrm{T}}[H_n P_n^-(H_n)^{\mathrm{T}} + R_{n-1}]^{-1}$

Covariance matching [c]: $S_n^- = \frac{\sum_{i=n-M+1}^{n} e_i^- e_i^{-\mathrm{T}}}{\psi_1}$, $R_n = S_n^- - H_n P_n^- H_n^{\mathrm{T}}$, $Q_n = K_n S_n^- K_n^{\mathrm{T}}$

State estimation update: $\hat{x}_n^+ = \hat{x}_n^- + K_n e_n^-$

State Error covariance update: $P_n^+ = (I - K_n H_n) P_n^-$

Step 4 Parameter posteriori estimation time update

Error innovation: $e_n^+ = y_n - g(\hat{x}_n^+, \hat{\theta}_n^-, I_{B,n})$

Kalman gain matrix: $L_n = J_n^-(C_n)^{\mathrm{T}}[C_n J_n^-(C_n)^{\mathrm{T}} + W_{n-1}]^{-1}$

Covariance matching [c]: $S_n^+ = \frac{\sum_{i=n-N+1}^{n} e_i^+ e_i^{+\mathrm{T}}}{\psi_2}$, $W_n = S_n^+ - C_n J_n^- C_n^{\mathrm{T}}$, $V_n = L_n S_n^+ L_n^{\mathrm{T}}$

Parameter estimation update: $\hat{\theta}_n^+ = \hat{\theta}_n^- + L_n e_n^+$

Parameter error covariance update: $J_n^+ = (I - L_n C_n) J_n^-$

Step 5 Time update

n=n+1, return to step 2.

[a] r_n, ν_n, ω_n are the independent, zero-mean, Gaussian noise processes of the covariance matrices Q, V, R/W *respectively*.

[b] Considering that the true parameters values of Li-ion battery cells change very slowly, the discrete formula of system parameters is modeled as constants with small white noise perturbation

[c] ψ_1 *and* ψ_2 are covariance matching windows.

TABLE VII
STEPS OF BATTERY PACK SOP ESTIMATION

Step 1 Initialization [a]

set $I_{\mathrm{chg},n}^{\min} = \max\left(I_{\mathrm{chg}}^{\mathrm{up}}, I_{\mathrm{chg},n}^{\mathrm{SoC}}\right)$, $I_{\mathrm{chg},n}^{\max} = 0$, $I_{\mathrm{dis},n}^{\max} = \min\left(I_{\mathrm{dis}}^{\mathrm{up}}, I_{\mathrm{dis},n}^{\mathrm{SoC}}\right)$, $I_{\mathrm{dis},n}^{\min} = 0$

Step 2 Peak current binary search

Estimated Peak discharge current: $\hat{I}_{B,n}^{\max} = (I_{\mathrm{dis},n}^{\max} + I_{\mathrm{dis},n}^{\min}) / 2$

Estimated Peak charge current: $\hat{I}_{B,n}^{\min} = (I_{\mathrm{chg},n}^{\max} + I_{\mathrm{chg},n}^{\min}) / 2$

Step 3 Voltage and average temperature iterative computations. For k = 1, 2 ,…, compute

Computing cells diffusion voltage:

$U_{D\_\mathrm{dis},n+k}^s = e^{-\frac{\Delta t}{R_{D,n}C_{D,n}}} U_{D\_\mathrm{dis},n+k-1}^s + R_{D,n}(1 - e^{-\frac{\Delta t}{R_{D,n}C_{D,n}}})\hat{I}_{B,n}^{\max}$;

$U_{D\_\mathrm{chg},n+k}^s = e^{-\frac{\Delta t}{R_{D,n}C_{D,n}}} U_{D\_\mathrm{chg},n+k-1}^s + R_{D,n}(1 - e^{-\frac{\Delta t}{R_{D,n}C_{D,n}}})\hat{I}_{B,n}^{\min}$;

$U_{D\_\mathrm{dis},n+k}^l = (\beta_{0,N}^l + \Delta t(k+n-N)\beta_{1,N}^l + \Delta t^2(k+n-N)^2\beta_{2,n}^l)U_{D\_\mathrm{dis},n+k}^s$;

$U_{D\_\mathrm{chg},n+k}^l = (\beta_{0,N}^l + \Delta t(k+n-N)\beta_{1,N}^l + \Delta t^2(k+n-N)^2\beta_{2,n}^l)U_{D\_\mathrm{chg},n+k}^s$;

Computing cells terminal voltage:

$U_{T,n+k}^{s,\mathrm{dis}} = U_{OC}^s(z_{\mathrm{dis},n}^p + \frac{\Delta t k \hat{I}_{B,n}^{\max}}{3600 \times C_N}) - U_{t,n+k}^{s,\mathrm{dis}} - R_{S,n}\hat{I}_{B,n}^{\max}$;

$U_{T,n+k}^{s,\mathrm{chg}} = U_{OC}^s(z_{\mathrm{dis},n}^p + \frac{\Delta t k \hat{I}_{B,n}^{\min}}{3600 \times C_N}) - U_{t,n+k}^{s,\mathrm{chg}} - R_{S,n}\hat{I}_{B,n}^{\min}$;

$U_{T,n+k}^{l,\mathrm{dis}} = U_{T,n+k}^{s,\mathrm{dis}} + U_{D,n+k}^{s,\mathrm{dis}} - U_{D,n+k}^{l,\mathrm{dis}} + \Delta U_{OC,N}^l + \Delta R_{S,N}^l \hat{I}_{B,n}^{\max}$;

$U_{T,n+k}^{l,\mathrm{chg}} = U_{T,n+k}^{s,\mathrm{chg}} + U_{D,n+k}^{s,\mathrm{chg}} - U_{D,n+k}^{l,\mathrm{chg}} + \Delta U_{OC,N}^l + \Delta R_{S,N}^l \hat{I}_{B,n}^{\min}$;

Computing battery pack average temperature:

$T_{P,n+k}^{\mathrm{dis}} = e^{-\frac{\Delta t k \alpha_1}{\alpha_2}} T_{P,n+k-1}^{\mathrm{dis}} + (1 - e^{-\frac{\Delta t k \alpha_1}{\alpha_2}}) \frac{(U_{OC,n}^p - U_{T,l}^p)\hat{I}_{B,n}^{\max} + h_p A_p T_{Air}}{a_2}$;

$T_{P,n+k}^{\mathrm{chg}} = e^{-\frac{\Delta t k \alpha_1}{\alpha_2}} T_{P,n+k-1}^{\mathrm{chg}} + (1 - e^{-\frac{\Delta t k \alpha_1}{\alpha_2}}) \frac{(U_{OC,n}^p - U_{T,l}^p)\hat{I}_{B,n}^{\min} + h_p A_p T_{Air}}{a_2}$

Step 4 Constraint check [b]

if $\min(U_{T\_\mathrm{dis},n+k}^s, U_{T\_\mathrm{dis},n+k}^l) < U_{\mathrm{lower}}^{\mathrm{up}} \,\|\, T_{P\_\mathrm{dis},n+k} > T_P^{\mathrm{up}}$:

$I_{\mathrm{dis},n}^{\max} = \hat{I}_{B,n}^{\max}$, then

if $\max(U_{T\_\mathrm{chg},n+k}^s, U_{T\_\mathrm{chg},n+k}^l) < U_{\mathrm{upper}}^{\mathrm{up}} \,\|\, T_{P\_\mathrm{chg},n+k} > T_P^{\mathrm{up}}$: $I_{\mathrm{chg},n}^{\min} = \hat{I}_{B,n}^{\min}$, then

if k=q: jump to step 5;

else: k=k+1, return to step 3.

Step 5 Convergence check and recursion [c]

if $I_{\mathrm{dis},n}^{\max} - I_{\mathrm{dis},n}^{\min} < \varepsilon$ & $I_{\mathrm{chg},n}^{\max} - I_{\mathrm{chg},n}^{\min} < \varepsilon$: jump to step 6.

else: $I_{\mathrm{dis},n}^{\min} = \hat{I}_{B,n}^{\max}$, $I_{\mathrm{chg},n}^{\max} = \hat{I}_{B,n}^{\min}$, return to step 2.

Step 6 Battery pack SoP estimation

$P_{\mathrm{dis},n}^p = \hat{I}_{B,n}^{\max} \times (U_{T,n+q}^{s,\mathrm{dis}} + \sum_{i=0}^{9k} U_{T,n+q}^{l,\mathrm{dis}})$; $P_{\mathrm{chg},n}^p = \hat{I}_{B,n}^{\min} \times (U_{T,n+q}^{s,\mathrm{chg}} + \sum_{i=0}^{9k} U_{T,n+q}^{l,\mathrm{chg}})$

[a] $I_{\mathrm{dis}}^{\mathrm{up}}$ and $I_{\mathrm{chg}}^{\mathrm{up}}$ are bounds of the cell operating current [43],

$I_{\mathrm{chg},n}^{\mathrm{SoC}} = 3600 \times C_N \frac{z_{\mathrm{chg},n}^p - 0.95}{q\Delta t}$, $I_{\mathrm{dis},n}^{\mathrm{SoC}} = 3600 \times C_N \frac{z_{\mathrm{dis},n}^p - 0.15}{q\Delta t}$.

[b] $U_{\mathrm{lower}}^{\mathrm{up}}$ and $U_{\mathrm{upper}}^{\mathrm{up}}$ are bounds of the cell operating voltage. T_P^{up} is the upper bound of the battery pack operating temperature, set $T_P^{\mathrm{up}} = 323.15\mathrm{K}$.

[c] ε is the peak current convergence radius, set ε=0.1A.

continuous interval and the pack temperature field is equally distributed at sample time t_n. Then, we use the dichotomy method to solve multiple equations to estimate the peak discharge/charge current of a battery pack. The details of the SoP estimation based on the battery inconsistent model and the thermal model are summarized in Table VII.

C. Fuzzy Logic Based Control Strategy

A Fuzz logic based EMS can be recognized as a combination of different control rules. Its performance is determined by fuzzy rules, fuzzy variables, and the shape of MFs. Generally, we can increase inputs and outputs the rule base EMS for a better performance. However, the increase of inputs and outputs will lead to an exponentially growing of the computing time and the control rule number. Therefore, we use the model prediction method to minimum the EMS input dimension first. Then, the designed DFLC solves power distributions between NCM pack, LTO pack and gasoline energy with a limited increase in calculation complexity by splitting this MIMO system into two series connected MISO systems. The schematic of the DFLC is shown in Fig. 6. Fuzzy logical controller 1 (FLC 1) is devoted to control the APU output power increment $\Delta P_{\mathrm{APU},n+1}$. The fuzzy variables of FLC 1 inputs are the APU output power $P_{\mathrm{APU},n}$ and the PHEV required power $P_{\mathrm{Req},n+1}$ predicted by (1)–(4). $P_{\mathrm{APU},n+1}$ is the sum of $\Delta P_{\mathrm{APU},n+1}$ and $P_{\mathrm{APU},n}$. Switch 1 is a

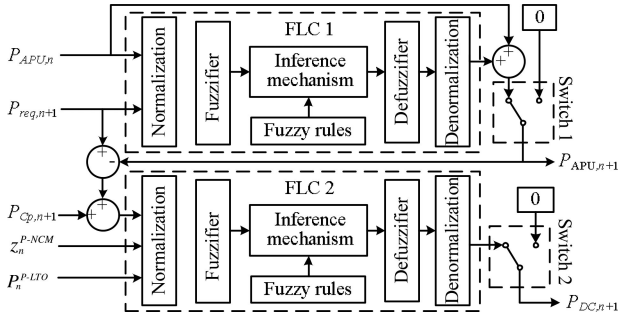

Fig. 6. Schematic of the DFLC.

logical component control by a state machine, which is used to distinguish whether the APU should be started-up or flamed-out. The exercising logic of Switch 1 in different hybrid driving mode is defined as follows.

1) *Charge-Depleting mode (CD mode):* when one of battery packs SoCs is less than 30% or $P_{\mathrm{dis},n}^{P-\mathrm{LTO}} + P_{\mathrm{dis},n}^{P-\mathrm{NCM}} < P_{\mathrm{Req},n+1}$, switch 1 would be triggered and the APU would be turn ON; when both battery packs SoCs are larger than 35% or gasoline is exhausted or $P_{\mathrm{chg},n}^{P-\mathrm{LTO}} + P_{\mathrm{chg},n}^{P-\mathrm{NCM}} > P_{\mathrm{Req},n+1}$, switch 1 would be triggered to 0 (Shut OFF the APU).
2) *Charge-Sustaining mode (CS mode):* when one of battery packs SoCs is larger than 80% or the fuel load is exhausted, the APU would be shut OFF; when both battery packs SoCs are less than 70%, the APU would be turn ON.

FLC 2 is applied to control the dc/dc converter output power $P_{\mathrm{DC},n+1}$. The input fuzzy variables of FLC 2 are HESS required power $P_{H,n+1}$, NCM pack SoC z_n^{P-NCM}, and LTO pack SoP $P_n^{P-\mathrm{LTO}}$. Generally, fuzzy-logic based EMS inputs are SoCs of the HESS. Since the maximum charge and discharge power of the NCM pack are small, we care more about the NCM pack residual energy than the power capability. Therefore, the NCM pack SoC is used as a FLC 2 input. The LTO pack is used to absorb high power fluctuations, but the SoC can only reflect its partial system states information. The SoP contains more system information than SoC, including the remaining capacity, the diffusion voltage and the power capability. Therefore, the LTO pack SoP is chosen as an input variable of the FLC 2. In addition, if $P_{H,n+1}$ is negative, the $z_n^{P-\mathrm{NCM}}$ and $P_n^{P-\mathrm{LTO}}$ are the charge SoC and charge SoP separately. Else, the inputs are the discharge SoC and discharge SoP. $P_{H,n+1}$ is defined as follows:

$$P_{H,n+1} = P_{\mathrm{Req},n+1} - P_{\mathrm{APU},n+1} + P_{Cp,n+1} \tag{20}$$

where $P_{Cp,n+1}$ is the power compensation for maintaining the SoC consistency between two packs, defined as follows:

$$P_{Cp,n+1} = \begin{cases} 48000(e^{z_n^{P-\mathrm{NCM}} - z_n^{P-\mathrm{LTO}}} - 1) & z_n^{P-\mathrm{NCM}} \geq z_n^{P-\mathrm{LTO}} \\ -48000(e^{z_n^{P-\mathrm{LTO}} - z_n^{P-\mathrm{NCM}}} - 1) & z_n^{P-\mathrm{NCM}} < z_n^{P-\mathrm{LTO}} \end{cases} \tag{21}$$

In considering the dc/dc converter poor efficiency under low loads, when $P_{\mathrm{DC},n+1}$ is within the range of ± 2 kw or the NCM pack SoC is below 15%, switch 2 would be triggered and the converter would be turned OFF to improve the HESS energy efficiency. If $P_{\mathrm{APU},n+1}$ and $P_{\mathrm{DC},n+1}$ are determined, the NCM pack output power can be calculated by (12) and the LTO pack output power is $P_{\mathrm{Req},n+1} - P_{\mathrm{APU},n+1} - P_{\mathrm{DC},n+1}$.

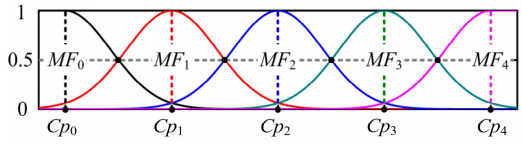

Fig. 7. Relationship between control-points and MFs.

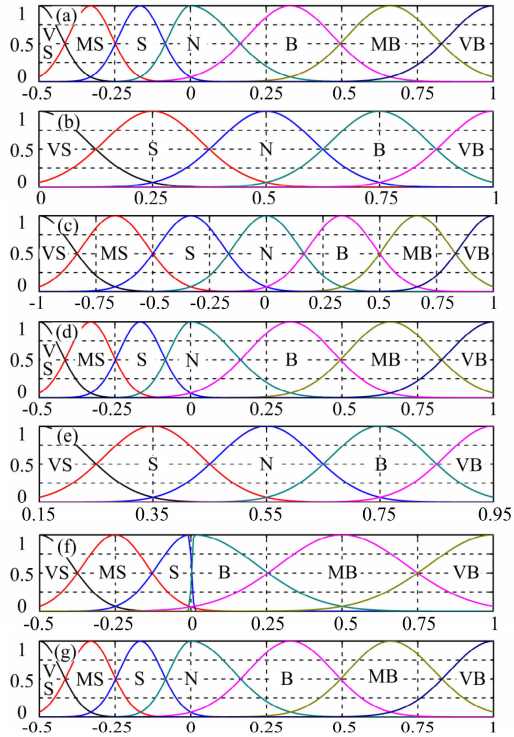

Fig. 8. MFs of fuzzy variables: (a) $P_{\mathrm{Req},n+1}$; (b) $P_{\mathrm{APU},n}$; (c) $\Delta P_{\mathrm{APU},n+1}$; (d) $P_{H,n+1}$; (e) $z_n^{P-\mathrm{NCM}}$; (f) $P_n^{P-\mathrm{LTO}}$; and (g) $P_{\mathrm{DC},n+1}$.

All fuzzy variables of DFLC are normalized to values between -1 and 1. Every fuzzy variable consists of a series of fuzzy subsets whose MFs are generated from control-point vector $\overrightarrow{Cp}$, as shown in Fig. 7, and as follows:

$$\mathrm{MF}_i(x) = \begin{cases} 2^{-\frac{4(x-Cp_i)^2}{(Cp_{i-1}-Cp_i)^2}} & x \leq Cp_i \\ 2^{-\frac{4(Cp_i-x)^2}{(Cp_i-Cp_{i+1})^2}} & x > Cp_i. \end{cases} \tag{22}$$

MFs of all fuzzy variables are shown in Fig. 8. The linguistic variables "VS, MS, S, M, B, MB, VB" of fuzzy subsets denote "very small, medium small, small, medium, big, medium big, and very big." The linguistic fuzzy rule of FLC 1 is defined as follows if $P_{\mathrm{Req},n+1}$ is "XX," $P_{\mathrm{APU},n}$ is "XX," then $\Delta P_{\mathrm{APU},n+1}$ is "XX." For FLC 2, it is defined as: if $P_n^{P-\mathrm{LTO}}$ is "XX," $z_n^{P-\mathrm{NCM}}$ is "XX" and $P_{H,n+1}$ is "XX," then $P_{\mathrm{DC},n+1}$ is "XX." Fuzzy rules for the DFLC is shown in Fig. 9. The design principle

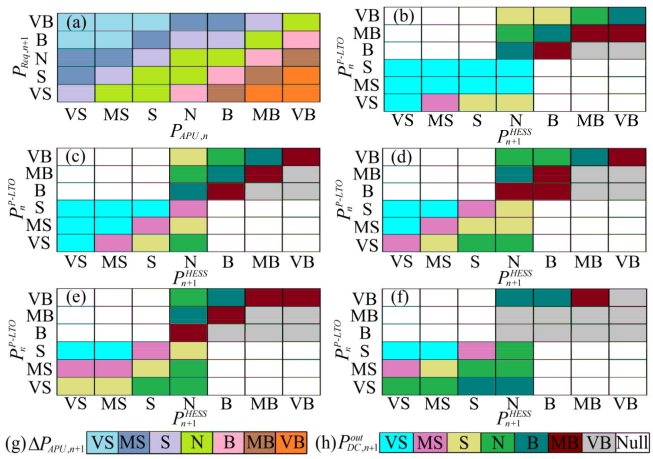

Fig. 9. (a) Fuzzy rules of (a) FLC 1. (b) FLC 2 when $z_n^{P-\mathrm{NCM}}$ is VS. (c) FLC 2 when $z_n^{P-\mathrm{NCM}}$ is S. (d) FLC 2 when $z_n^{P-\mathrm{NCM}}$ is *N*. (e) FLC 2 when $z_n^{P-\mathrm{NCM}}$ is B. (f) FLC 2 when $z_n^{P-\mathrm{NCM}}$ is VB. (g) Linguistic variable color-bar of FLC 1 output. (h) Linguistic variable color-bar of FLC 2 output.

for fuzzy rules is to maintain the APU working at the lowest BSFC operating area and keeping a high SoP of the LTO pack.

IV. Multiobjective Optimization for EMS

In this section, the NSGA-II optimization based on a MIL simulation approach is proposed to tune MFs of the EMS. The optimal objects are improving the target PHEV energy economy, minimizing battery packs capacity fades, minimizing the degradation inconsistency between two packs, and minimizing the PHEV driving cost unit distance.

A. Framework of MIL Simulation Approach

In order to quantize the PHEV dynamic performance with different EMS, which have no analytic expression, a MIL framework is proposed to evaluate different EMSs as presented in Fig. 10.

Before, we start the MIL simulation, the first step is configuring the runtime environment of target PHEV model, including the initial fuel load, battery packs SoCs, driving cycles, and MFs of fuzzy variables. The APU and the dc/dc are turned OFF, all cells in-pack are well balanced with no SoC inconsistency and all cells diffusion voltage is 0 V.

During the MIL simulation process, according to the injected driving cycles and the established PHEV dynamic model, we can predict the PHEV required power at t_{n+1}. Then, SoC/SoP estimators process the NCM pack SoC and the LTO pack SoP at simulation time t_n based on cell voltages and currents fed back from last simulation period t_{n-1}. With all inputs being prepared, the power flows of the PHEV power system at next simulation time ($P_{\mathrm{APU},n+1}$, $P_{\mathrm{DC},n+1}$, $P_{\mathrm{LTO},n+1}$ and $P_{\mathrm{NCM},n+1}$) can be calculated by the DFLC and the dc/dc efficiency model. Then, $P_{\mathrm{LTO},n+1}$ and $P_{\mathrm{NCM},n+1}$ are transmitted to cell simulation models for simulating cells terminal voltages. A novel BP neural network based cell simulation model is used to simulate cell dynamic performance. The maximum output errors of cell simulation models are less than 3 mV and the number of neurons is minimized to reduce MIL simulation time and space complexity. The network consists one input layer, two hidden layers, and one output layer. The neuron numbers of each layer are 25, 80, 40, and 1, respectively. Network inputs are cell terminal voltage at t_n, cell output power at t_n, cell required power at t_{n+1}, cell temperature at t_n, and cell SoC at t_n. Cell terminal voltages at t_{n+1} is the network output. Each battery pack is assigned with five different networks, one of which is used as the simulation model for the selected cell, and the other four networks are randomly assigned to simulate unselected cells in-pack.

The MIL simulation step size is set to 0.5 s. If the fuel load is exhausted and one of pack SoCs is below 15%, the MIL simulation would be terminated and export evaluation indexes, which represent the individual fitness for NSGA-II optimization. Quantifiable evaluation functions are essential to compare the performance of different EMS. The LTO pack capacity fade rate $Q^{\mathrm{LTO}}_{\mathrm{Loss},N}$, the NCM pack capacity fade rate $Q^{\mathrm{NCM}}_{\mathrm{Loss},N}$ and the PHEV overall travelled distance D_N in MIL simulation are selected to calculate fitness functions:

$$f1 = \frac{Q^{\mathrm{NCM}}_{\mathrm{Loss},N} + 2.5Q^{\mathrm{LTO}}_{\mathrm{Loss},N}}{D}, \quad f2 = \left| \ln \frac{Q^{\mathrm{NCM}}_{\mathrm{Loss},N}}{Q^{\mathrm{LTO}}_{\mathrm{Loss},N}} \right|$$
$$f3 = \frac{1}{D_N} \tag{23}$$

where $f1$ evaluates the degradation rate of the HESS with the weights determined by the unit capacity depreciation expenses of different battery packs. $f2$ is applied to measure the degradation rate inconsistency between two battery packs. Since both NCM pack and LTO pack are placed in one battery module. If one of the battery pack reaches its cycle life, the entire HESS must be replaced. $f3$ can directly reflects the PHEV energy economy.

B. NSGA-II Based EMS Multiobjective Optimization

The EMS optimization problem is formulated as tuning the MFs of DFLC fuzzy subsets. The total number of parameters needed to be tuned for MFs is 44. NSGA-II is a heuristic search approach for solving multiparameter multiobjective optimization problems that is not suitable for standard optimization algorithms [44], and it can effectively avoid trapping in a local optimum solution. The optimization target is to minimize (23) globally. The flow diagram of the EMS optimization is shown in Fig. 11. The maximum population number of NSGA-II is set to 200 and the population size is set to 600.

A series of constraints are set to speed up NSGA-II convergence, including the maximum APU output power, the cells' operating voltages and operating currents shown in Tables I and II. Once these constraints are triggered, it indicates that the optimized EMS has defects of potential safety problems and large constants will be added to fitness functions as the penalty function. To avoid generating defective MFs, a lower bound and upper bound is set to restrict control-points in a valid range. In each generation loop, a new generation breeds from parent generation by simulated binary crossover and polynomial mutation approach. The fitness functions of each individual are

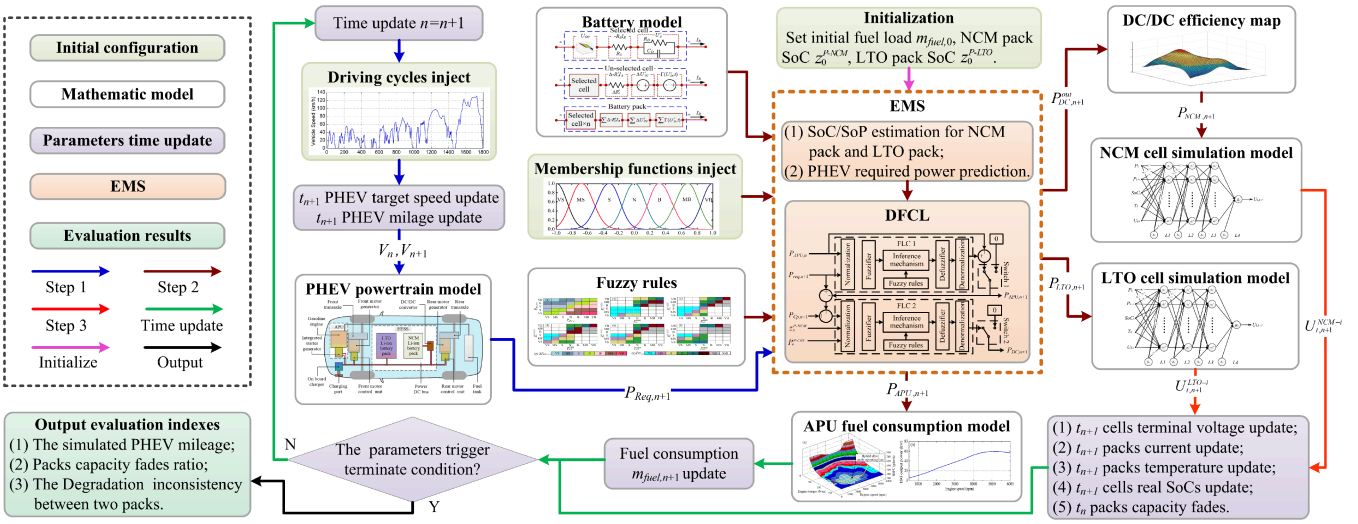

Fig. 10. Schematic of the MIL for EMS simulation.

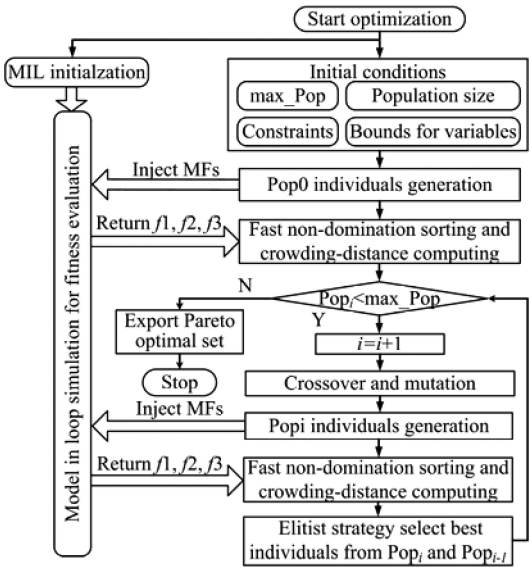

Fig. 11. Flow diagram of the NSGA-II based multiobjective optimization for the EMS.

evaluated in the MIL simulation process. Then, the Pareto salutation and crowding-distance of each individual, which are used to rank individuals, are computed based on fast nondomination sorting. Then, best individuals from Pop_i and Pop_{i-1} are selected by elitist strategy to compose a new parent generation. The algorithm repeatedly modifies individuals through selection, crossover, and mutation to move the population "evolve" toward an optimal solution.

The training drive cycle used in MIL simulation process is worldwide light-duty test cycle (WLTC). The PHEV initial fuel load is set to 1.5 kg and battery pack SoCs are set to 95% in CD mode; the initial fuel load is 4 kg and battery pack SoCs are 15% in CS mode. Fig. 12(a) and (b) shows the Pareto solution set of the optimized EMSs for different hybrid mode. In order to select the optimal solution from the Pareto solution set, unit distance driving cost contour lines based on gasoline/electricity cost and HESS depreciation cost were drawn and minimize the unit distance driving cost is taken as the fourth optimal object. At last, the individual owning the minimum unit distance driving cost is selected from the solution set of $f2 < 0.01$. Fig. 12(c) and (d) shows the tuned MFs for CD/CS modes.

V. Verification and Analysis

A. Framework of HIL Test Bench

In order to verify the EMSs performances in the embedded system, a HIL test bench shown in Fig. 13 is assembled.

Development platforms on host PC are LabVIEW and MATLAB. The LabVIEW platform is used to analytic CAN bus information, call MATLAB script, control the executing device, and display as a graphical user interface. MATLAB script periodic invokes a virtual PHEV powertrain modeled by Advisor. Then, simulation results are sent to the executing device and transformed into analog signals. The executing device contains a resistor card and a 12-channel battery cell simulator. The resistor card simulates performances of 10 NTC temperature sensors and four hall current sensors. Five channels of the battery cell simulator are used to simulate the terminal voltage of NCM cells and five channels are used to simulate LTO cells. The cell terminal voltages and temperatures are measured at sampling frequency of 20 Hz by the battery monitor unit (BMU) we developed, which is controlled by S12G series from Freescale and LTC68xx series from ADI. The measured results are transferred through the CAN bus to the battery control unit (BCU) that we developed, which is controlled by AURIX-2G series from Infineon. Both current sampling and packs' SoC and SoP estimations are served by BCU in real time. The PHEV power requirement is calculated by ADVISOR models in real time. Then, the PHEV required power transferred to the BCU through CAN bus and the EMS programmed in BCU calculates the power distributions for the powertrain. Power distributions are fed back

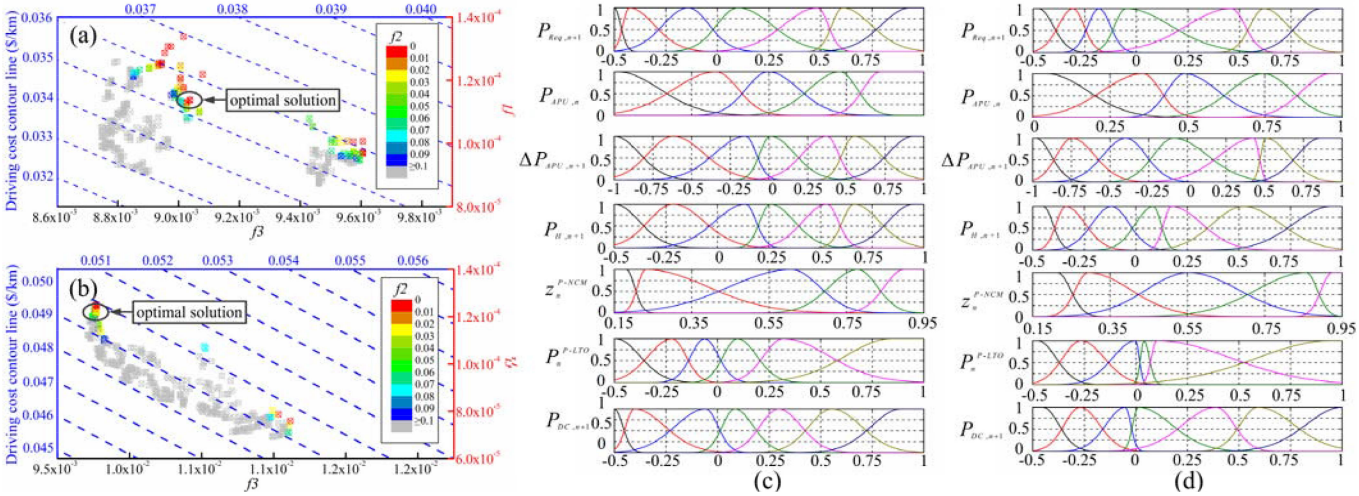

Fig. 12. Optimal results solved by NSGA-II. (a) The Pareto set of the EMS for CD mode. (b) The Pareto set of the EMS for CS mode. (c) The tuned MFs for CD mode. (d) The tuned MFs for CS mode.

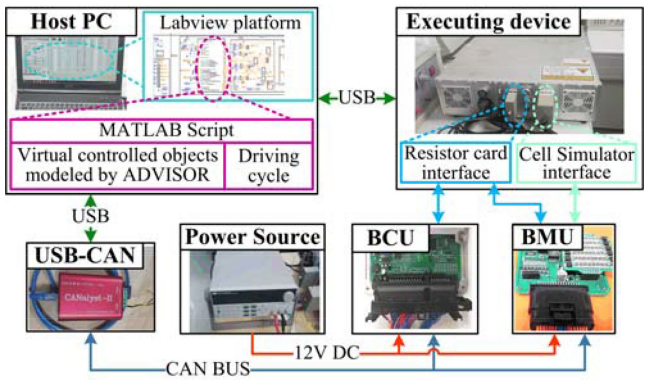

Fig. 13. HIL test bench configuration.

to ADVISOR models. In real car system, the required power can be determined by the accelerator pedal position.

B. DP-Based EMS for Comparison

A DP-based EMS as an approximate optimal EMS for the test-driving cycle is applied to verify the performance of the EMS optimized by NSGA-II. DP is an optimization approach that recursively transforms a complex problem into a sequence of simpler multistage problems. The energy management problem in our article can be regarded as a 1-D and 2-D combined resource allocation problem, and it is formulated based on the inverse order method as follows:

$$Z = \sum_{n=1}^{N} \left[g_1(u_n, s_n) + g_2(u_n, s_n) \right] \tag{24}$$

$$s_n = \left[z_n^{P-\mathrm{NCM}} \; U_{D,n}^{P-\mathrm{NCM}} \; Q_{\mathrm{Loss},n}^{\mathrm{NCM}} \; z_n^{P-\mathrm{LTO}} \; U_{D,n}^{P-\mathrm{LTO}} \; Q_{\mathrm{Loss},n}^{\mathrm{LTO}} \; m_{\mathrm{Fuel},n} \; P_{\mathrm{APU},n} \right]^{\mathrm{T}} \tag{25}$$

$$u_n = \left[I_{B,n}^{\mathrm{NCM}} \; \Delta P_{\mathrm{APU},n} \right] \tag{26}$$

$$s_{n+1} = F(s_n, u_n, I_{B,n}^{\mathrm{LTO}}, P_{\mathrm{Req},n}) \tag{27}$$

$$\begin{cases} g_1(u_n, s_n, \Delta D_n) = w_1 \frac{\Delta D_n}{\Delta Q_{\mathrm{Loss},n}^{\mathrm{NCM}} + 2.5 \Delta Q_{\mathrm{Loss},n}^{\mathrm{LTO}}} \\ g_2(u_n, s_n) = -w_2 \left| \ln \frac{Q_{\mathrm{Loss},n}^{\mathrm{NCM}}}{Q_{\mathrm{Loss},n}^{\mathrm{LTO}}} \right| \\ g_3(u_n, s_n, I_{B,n}^{\mathrm{LTO}}, P_{\mathrm{Req},n}) = w_3 \left(\frac{0.25}{\Delta m_{\mathrm{Fuel},n}} + \frac{P_n^{\mathrm{LTO}} + P_n^{\mathrm{NCM}}}{P_{\mathrm{Req},n} - P_{\mathrm{APU},n}} \right) \end{cases} \tag{28}$$

$$\begin{aligned} &(I_{B,n}^{\mathrm{LTO}})^2 R_{S,n}^{P-\mathrm{LTO}} - I_{B,n}^{\mathrm{LTO}} [U_{\mathrm{OC},n}^{P-\mathrm{LTO}}(z_n^{P-\mathrm{LTO}}) - U_{D,n}^{P-\mathrm{LTO}}] \\ &- \left[P_{\mathrm{Req},n} - P_{\mathrm{APU},n} - U_{T,n}^{P-\mathrm{NCM}} I_{B,n}^{\mathrm{NCM}} \eta_{\mathrm{DC}}^{*}(I_{B,n}^{\mathrm{NCM}}, U_{T,n}^{P-\mathrm{NCM}}) \right] \\ &= 0 \end{aligned} \tag{29}$$

where maximum Z is the optimal object, N is the total recursion steps, g_1, g_2, and g_3 are evaluate functions, w_1, w_2, and w_3 are weight coefficients, s_n is the state vector, u_n is the control strategy, η_{DC}^{*} is a revised dc/dc efficiency model, $I_{B,n}^{\mathrm{LTO}}$ can be solved by (29), and (27) is the state transfer equation of the powertrain which can be derived based on the battery state-space model, pack degradation model, and BSFC map. Here, we set $Q_{\mathrm{Loss},N} = 0$, $Q_{\mathrm{Loss},n-1} = Q_{\mathrm{Loss},n} + \Delta Q_{\mathrm{Loss},n}$, and $m_{\mathrm{Fuel},N} = 0$. When the APU is turned OFF, $P_{\mathrm{APU},n} = \Delta P_{\mathrm{APU},n} = 0$ and the energy management problem degrades into a single resource allocation problem. DP-based EMS is developed to find the optimal control vector $U = [u_1, u_2, \ldots, u_N]$ to maximize the (24), while satisfying to the constraints as follows:

$$\begin{aligned} I_{B,n}^{\mathrm{NCM}} \in &\left(\frac{3600 C_P^{\mathrm{NCM}} (z_n^{P-\mathrm{NCM}} - 0.95)}{\Delta t}, \right. \\ &\left. \frac{3600 C_P^{\mathrm{NCM}} (z_n^{P-\mathrm{NCM}} - 0.15)}{\Delta t} \right) \\ &\cap \left(\frac{P_{\mathrm{Req},n} - I_{\max,n}^{\mathrm{LTO}} U_{T,n}^{\mathrm{LTO}}}{U_{T,n}^{\mathrm{NCM}}}, \frac{P_{\mathrm{Req},n} - I_{\min,n}^{\mathrm{LTO}} U_{T,n}^{\mathrm{LTO}}}{U_{T,n}^{\mathrm{NCM}}} \right) \\ &\cap (-45, -7) \cup (7, \; 90) \end{aligned}$$

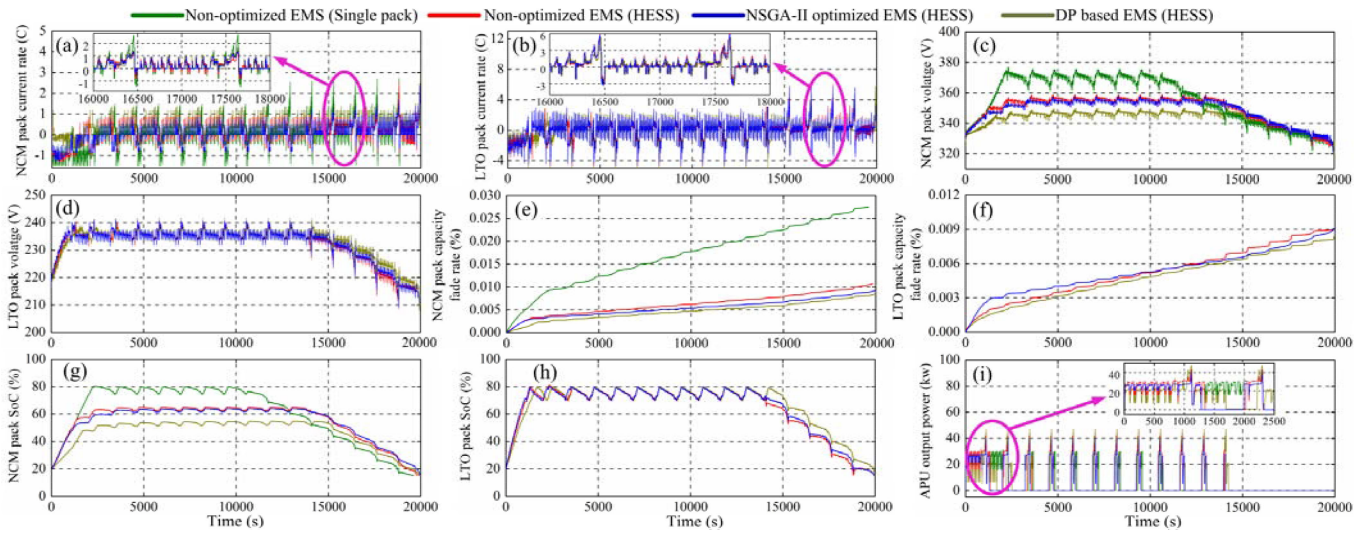

Fig. 14. HIL test results in CS mode. (a) NCM pack current rate. (b) LTO pack current rate. (c) NCM pack terminal voltage. (d) LTO pack terminal voltage. (e) NCM pack capacity fade rate. (f) LTO pack capacity fade rate. (g) NCM pack SoC variation curve. (h) LTO pack SoC variation curve. (i) APU output power curve.

$$\Delta P_{\mathrm{APU},n} \in (-20000, 20000) \cap (5257 - P_{\mathrm{APU},n}, 59647 - P_{\mathrm{APU},n})$$

$$I^{\mathrm{LTO}}_{\max,n} \in \left(\frac{3600 C_P^{\mathrm{LTO}} (z_n^{P-\mathrm{LTO}} - 0.95)}{\Delta t}, \frac{3600 C_P^{\mathrm{LTO}} (z_n^{P-\mathrm{LTO}} - 0.15)}{\Delta t} \right) \cap (-240,\ 300).$$

The DP-based EMS recurrence relation can be described as

$$\begin{aligned} & f(u_n, s_n, I^{\mathrm{LTO}}_{B,n}, P_{\mathrm{Req},n}, \Delta D_n) \\ &= \max[g_{P,1}(u_n, s_n, \Delta D_n) + g_{P,2}(u_n, s_n) \\ &\quad + g_{P,3}(u_n, s_n, I^{\mathrm{LTO}}_{B,n}, P_{\mathrm{Req},n})] \end{aligned} \tag{30}$$

$$\begin{aligned} & f(u_k, s_k, I^{\mathrm{LTO}}_{B,k}, P_{\mathrm{Req},k}, \Delta D_k) \\ &= \max[g_{P,1}(u_k, s_k, \Delta D_k) + g_{P,2}(u_k, s_k) \\ &\quad + g_{P,3}(u_k, s_k, I^{\mathrm{LTO}}_{B,k}, P_{\mathrm{Req},k}) \\ &\quad + f(u_{k+1}, s_{k+1}, I^{\mathrm{LTO}}_{B,k+1}, P_{\mathrm{Req},k+1}, \Delta D_{k+1})] \end{aligned} \tag{31}$$

where $k = 1, 2, \ldots, n-1$; $g_{P,1}, g_{P,2},$ and $g_{P,3}$ are the Pareto solution set of $g_1, g_2,$ and g_3, respectively; and $f(s_n)$ is the evaluation function. Equations (30) and (31) are solved by the sparse dense method. Every elements in u_n are linearly discretized into 32 numerical values between its constraints at every time step. The time step Δt of DP approach is set to 0.5 s and the length of the N is 40000.

The driving cycle used in DP approach is the NEDC cycle and the initial setting of the PHEV powertrain is the same as the HIL test sets. The generated control vector $U$is saved as a table in the BCU, and BCU outputs u_n periodically to carry out the HIL test for DP-based EMS.

C. HIL Test Results Analysis

The verification driving cycle loaded in HIL tests is the NEDC cycle, which owns a certain resemblance to WLTC. The WLTC cycle represents PHEV historical driving data. The HIL time step is 0.05 s for NSGA-II optimized EMSs and 0.5 s for DP-based EMSs. HIL test results in CS mode are given in Fig. 14. The PHEV initial fuel load is 7 kg. To guarantee the same initial electric energy be stored, the initial SoC of the archetypal NCM pack is 19.1% and the initial SoCs of two packs in HESS are both 20%.

Fig. 14(a) indicates that the HESS can effectively reduce the NCM pack peak current rate, and the NCM pack outputs current in a smooth way without surge impact when using the NSGA-II optimized EMS. Therefore, the dc/dc converter is maintained in a high efficiency area and the NCM pack capacity fade rate is reduced by 13.0% as shown in Fig. 14(e). The LTO pack current rate in Fig. 14(b) is reduced nonsignificantly by the NSGA-II optimized EMS, resulting in a slight reduction of the LTO pack capacity fade rate as shown in Fig. 14(f). Fig. 15(c) and (d) is pack voltages measure by the BMU. Comparing Fig. 14(g) with (h), the NCM pack SoC in HESS is sustained smoothly at a low level, while the LTO pack SoC fluctuates sharply between 75%–80%, which verifies the LTO pack absorbing power fluctuation as expected. In Fig. 15(i), the APU using the optimized EMS owns a less power fluctuation than the nonoptimized EMS, which contributes to lower the fuel consumption caused by power fluctuation.

The mileage of the PHEV with a single NCM pack is 180.0 km and the mileage of the PHEV with HESS is extended to 184.5 km when using the NSGA-II optimized EMS and it is 186.6 km when using the DP-based EMS. The energy economy improvement of the optimized EMS is 2.5%, and the improvement is 3.6% of the DP-based EMS. The unit distance capacity fade rates of the PHEV energy storage systems (ESS) are 1.53 $\times$ 10^{-4}%/km with the nonoptimized EMS (Single pack), 5.9

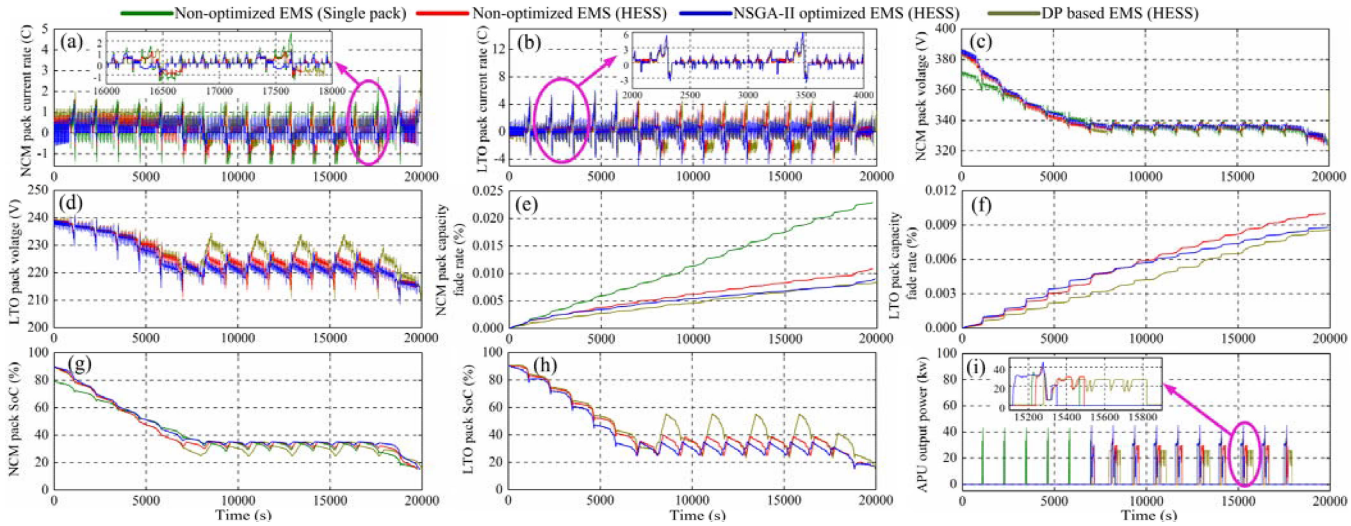

Fig. 15. HIL test results in CD mode. (a) NCM pack current rate. (b) LTO pack current rate. (c) NCM pack terminal voltage. (d) LTO pack terminal voltage. (e) NCM pack capacity fade rate. (f) LTO pack capacity fade rate. (g) NCM pack SoC variation curve. (h) LTO pack SoC variation curve. (i) APU output power variation curve.

TABLE VIII
SUMMARY OF HIL TEST RESULTS

	CS mode			CD mode		
	Q_{Loss}^{NCM}/D (%/km)	Q_{Loss}^{LTO}/D (%/km)	D (km)	Q_{Loss}^{NCM}/D (%/km)	Q_{Loss}^{LTO}/D (%/km)	D (km)
Non-optimized EMS (single pack)	1.53×10^{-4}	--	180.0	1.27×10^{-4}	--	181.5
Non-optimized EMS (HESS)	5.88×10^{-5}	4.90×10^{-5}	182.7	6.01×10^{-5}	5.51×10^{-5}	181.3
NSGA-II Optimized EMS (HESS)	5.05×10^{-5}	4.93×10^{-5}	184.5	4.91×10^{-5}	4.77×10^{-5}	184.0
DP base EMS (HESS)	4.59×10^{-5}	4.55×10^{-5}	186.6	4.63×10^{-5}	4.65×10^{-5}	186.6

$\times\ 10^{-5}$%/km with the nonoptimized EMS, $5.0\ \times\ 10^{-5}$%/km with the optimized EMS, and 4.5×10^{-5}%/km with the DP-based EMS. It is stipulated when capacity fade rate of any one pack in ESS is larger than 20%, the ESS reaches the end of its cycle life and the whole ESS should be replaced. With the CD mode HIL test results summarized in Table VII, we extrapolate ideally that, when using the optimized EMS, the ESS cycle life is improved by 16.5% in comparison with the nonoptimized EMS (HESS) and improved by 203% in comparison with the archetypal PHEV with a single NCM pack. When using the DP-based EMS, the corresponding improvement is 233%.

The HIL test results in CD mode are given in Fig. 15. The PHEV initial fuel load is 4 kg. The initial SoC of the archetypal NCM pack is 79.4% and the initial SoCs of packs in HESS are both 90%. Fig. 15(a) and (b) shows the NCM/LTO pack current rate of different EMSs. The NSGA-II optimized EMS brings an obvious reduction to battery pack current rates. As a result, the NCM pack capacity fade rate in the HESS is reduced by 17.2% in comparison with the nonoptimized EMS (HESS) as shown in Fig. 15(e), and it is reduced by 12.0% of the LTO pack as shown in Fig. 15(f). Fig. 15(c) and (d) shows battery packs voltage measure by BMU. Comparing Fig. 15(g) and (h), SoCs of NCM pack are sustained between 30% and 35%, while LTO pack SoCs fluctuate sharply between 25% and 40% after APU first start-up. In Fig. 15(i), the optimized EMS and DP-based EMS can maintain the APU working in high efficient areas longer and more steady than the nonoptimized EMS.

When using the nonoptimized EMS, the mileage of the PHEV is 181.5 km with a single NCM pack and it is 181.3 km with HESS. Because of employing a dc/dc converter, the energy conversion loss in a HESS is larger than a single NCM pack, which results to the PHEV mileage regression. If the HESS is not matched up with an appropriate EMS, certain performances of the PHEV with HESS may be inferior to the archetypal PHEV. The PHEV mileage is extended to 184.0 km by using the optimized EMS and it is 186.6 km when using the DP-based EMS. Therefore, in comparison with the archetypal PHEV, the energy efficiency improvement of the PHEV with HESS is 1.6% when using the optimized EMS and it is 2.9% when using the DP-based EMS. With the CS mode HIL test results summarized in Table VII, when using optimized EMS, the ideal PHEV ESS cycle life is improved by 22.4% in comparison with the nonoptimized EMS (HESS) and it is improved by 159% in comparison with the archetypal PHEV. When using the DP-based EMS, the corresponding improvement is 173%.

The HIL test results indicate that the HESS has a significant improvement on the cycle life of the PHEV ESS and NSGA-II optimized EMS performances on the ESS life span extension are close to DP-based offline optimal solutions. Since DP-based EMSs reduce the phenomenon of repeatedly energy exchanges

within the HESS and maintain the APU steadily working in high efficient areas, their performances are superior to NSGA-II optimized EMS. However, the driving cycle for DP-based EMS cannot be changed for online application. Otherwise, the DP-based EMS is completely ineffective, while NSGA-II optimized EMSs, which are optimized under the WLTC cycle, still brings substantial improvement of the PHEV performance under the NEDC cycle. In addition, although the HESS manufacturing cost is about 1.8–2.0 times higher than the archetypal NCM pack, the depreciation cost unit distance of the HESS is significantly lower than the archetypal NCM pack. Consequently, it seems practicable to improve the PHEV performance with its historical driving data by applying the optimization approach, we proposed in cloud computing center.

VI. Conclusion

In this article, a model prediction and fuzzy logic based EMS design and optimization framework is proposed for a PHEV with a HESS. In general, the conclusions can be drawn as follows:

1) A DAEKF and sliding least square method based dual timescale SoC estimation approach was proposed for battery packs with inconsistency. An innovative SoP estimator considering thermal constraints was proposed to predict the authentic battery pack power capability.
2) An innovative model prediction and a DFLC-based EMS framework was developed. Then, a systematic multiobjective optimization approach integrated by NSGA-II and MIL simulation was proposed for EMS optimization. The design of the EMS and the optimization approach has an important theoretical significance and engineering applications for improving PHEV energy economy, extend HESS life span, guiding EMSs designs for the PHEV as well.
3) A novel HIL test bench for EMSs performance verification was designed. HIL test results indicated that the HESS has a significant improvement on the cycle life of the ESS. EMSs optimized by WLTC are still practicable for further extension to the HESS cycle life and improving the PHEV energy efficiency under NEDC.

Our future work will focus on the influence of battery aging on EMS performance and develop a reinforce learning based EMS for continues improvement.

References

[1] S. Rivera and B. Wu, "Electric vehicle charging station with an energy storage stage for split-DC bus voltage balancing," *IEEE Trans. Power Electron.*, vol. 32, no. 3, pp. 2376–2386, Mar. 2017.

[2] H. Fathabadi, "Plug-In hybrid electric vehicles: Replacing internal combustion engine with clean and renewable energy based auxiliary power sources," *IEEE Trans. Power Electron.*, vol. 33, no. 11, pp. 9611–9618, Nov. 2018.

[3] M. Noori, S. Gardner, and O. Tatari, "Electric vehicle cost, emissions, and water footprint in the United States: Development of a regional optimization model," *Energy*, vol. 89, pp. 610–625, Sep. 2015.

[4] K. W. E. Cheng, B. P. Divakar, H. J. Wu, K. Ding, and F. H. Ho, "Battery-management system (BMS) and SOC development for electrical vehicles," *IEEE Trans. Veh. Technol.*, vol. 60, no. 1, pp. 76–88, Jan. 2011.

[5] D. Y. Huang, Z. Chen, C. W. Zheng, and H. B. Li, "A model-based state-of-charge estimation method for series-connected lithium-ion battery pack considering fast-varying cell temperature," *Energy*, vol. 185, pp. 847–861, Oct. 2019.

[6] A. Emadi, K. Rajashekara, S. S. Williamson, and S. M. Lukic, "Topological overview of hybrid electric and fuel cell vehicular power system architectures and configurations," *IEEE Trans. Veh. Technol.*, vol. 54, no. 3, pp. 763–770, May 2005.

[7] Y. J. Xing, W. He, M. Pecht, and K. L. Tsui, "State of charge estimation of lithium-ion batteries using the open-circuit voltage at various ambient temperatures," *Appl. Energy*, vol. 113, pp. 106–115, Jan. 2014.

[8] G. Suri and S. Onori, "A control-oriented cycle-life model for hybrid electric vehicle lithium ion batteries," *Energy*, vol. 96, pp. 644–653, Feb. 2016.

[9] N. Omar *et al.*, "Lithium iron phosphate based battery-Assessment of the aging parameters and development of cycle life model," *Appl. Energy*, vol. 113, pp. 1575–1585, Jan. 2014.

[10] J. Liu and Z. Q. Chen, "Remaining useful life prediction of lithium-ion batteries based on health indicator and gaussian process regression model," *IEEE Access*, vol. 7, pp. 39474–39484, 2019.

[11] M. Jafari, A. Gauchia, K. L. Zhang, and L. Gauchia, "Simulation and analysis of the effect of real-world driving styles in an EV battery performance and aging," *IEEE Trans. Transp. Electrific.*, vol. 1, no. 4, pp. 391–401, Dec. 2015.

[12] S. M. Lukic, S. G. Wirasingha, F. Rodriguez, J. Cao, and A. Emadi, "Power management of an ultracapacitor/battery hybrid energy storage system in an HEV," in *Proc. IEEE Veh. Power Propulsion Conf.*, 2006, pp. 179–184.

[13] Z. Y. Chen, R. Xiong, and J. Y. Cao, "Particle swarm optimization-based optimal power management of plug-in hybrid electric vehicles considering uncertain driving conditions," *Energy*, vol. 96, pp. 197–208, Feb. 2016.

[14] C. G. Hochgraf, J. K. Basco, T. P. Bohn, and I. Bloom, "Effect of ultracapacitor-modified PHEV protocol on performance degradation in lithium-ion cells," *J. Power Sour.*, vol. 246, pp. 965–969, Jan. 2014.

[15] H. M. Liu, Z. X. Wang, J. Cheng, and D. Maly, "Improvement on the Cold cranking capacity of commercial vehicle by using supercapacitor and lead-acid battery hybrid," *IEEE Trans. Veh. Technol.*, vol. 58, no. 3, pp. 1097–1105, Mar. 2009.

[16] J. Cao and A. Emadi, "A new battery/ultracapacitor hybrid energy storage system for electric, hybrid, and plug-in hybrid electric vehicles," *IEEE Trans. Power Electron.*, vol. 27, no. 1, pp. 122–132, Jan. 2012.

[17] H. L. Yu, D. Tarsitano, X. S. Hu, and F. Cheli, "Real time energy management strategy for a fast charging electric urban bus powered by hybrid energy storage system," *Energy*, vol. 112, pp. 322–331, Oct. 2016.

[18] A. Burke and M. Miller, "The power capability of ultracapacitors and lithium batteries for electric and hybrid vehicle applications," *J. Power Sour.*, vol. 196, no. 1, pp. 514–522, Jan. 2011.

[19] J. Y. Shen, S. Dusmez, and A. Khaligh, "Optimization of sizing and battery cycle life in battery/ultracapacitor hybrid energy storage systems for electric vehicle applications," *IEEE Trans. Ind. Informat.*, vol. 10, no. 4, pp. 2112–2121, Nov. 2014.

[20] R. Carter, A. Cruden, and P. J. Hall, "Optimizing for efficiency or battery life in a battery/supercapacitor electric vehicle," *IEEE Trans. Veh. Technol.*, vol. 61, no. 4, pp. 1526–1533, May 2012.

[21] B. Kang and G. Ceder, "Battery materials for ultrafast charging and discharging," *Nature*, vol. 458, no. 7235, pp. 190–193, Mar. 2009.

[22] A.-A. Mamun, Z. F. Liu, D. M. Rizzo, and S. Onori, "An integrated design and control optimization framework for hybrid military vehicle using lithium-ion battery and supercapacitor as energy storage devices," *IEEE Trans. Transp. Electrific.*, vol. 5, no. 1, pp. 239–251, Mar. 2019.

[23] R. Wegmann, V. Doge, and D. U. Sauer, "Assessing the potential of a hybrid battery system to reduce battery aging in an electric vehicle by studying the cycle life of a graphite vertical bar NCA high energy and a LTO vertical bar metal oxide high power battery cell considering realistic test profiles," *Appl. Energy*, vol. 226, pp. 197–212, Sep. 2018.

[24] Z. Y. Song, H. Hofmann, J. Q. Li, X. B. Han, and M. G. Ouyang, "Optimization for a hybrid energy storage system in electric vehicles using dynamic programing approach," *Appl. Energy*, vol. 139, pp. 151–162, Feb. 2015.

[25] Z. Y. Song, H. Hofmann, J. Q. Li, J. Hou, X. W. Zhang, and M. G. Ouyang, "The optimization of a hybrid energy storage system at subzero temperatures: Energy management strategy design and battery heating requirement analysis," *Appl. Energy*, vol. 159, pp. 576–588, Dec. 2015.

[26] F. R. Salmasi, "Control strategies for hybrid electric vehicles: Evolution, classification, comparison, and future trends," *IEEE Trans. Veh. Technol.*, vol. 56, no. 5, pp. 2393–2404, Sep. 2007.

[27] J. P. Trovao, P. G. Pereirinha, H. M. Jorge, and C. H. Antunes, "A multi-level energy management system for multi-source electric vehicles-An integrated rule-based meta-heuristic approach," *Appl. Energy*, vol. 105, pp. 304–318, May 2013.
[28] N. J. Schouten, M. A. Salman, and N. A. Kheir, "Energy management strategies for parallel hybrid vehicles using fuzzy logic," *Control Eng. Pract.*, vol. 11, no. 2, pp. 171–177, Feb. 2003.
[29] M. Zandi, A. Payman, J. P. Martin, S. Pierfederici, B. Davat, and F. Meibody-Tabar, "Energy management of a fuel cell/supercapacitor/battery power source for electric vehicular applications," *IEEE Trans. Veh. Technol.*, vol. 60, no. 2, pp. 433–443, Feb. 2011.
[30] Y. H. Hung and C. H. Wu, "An integrated optimization approach for a hybrid energy system in electric vehicles," *Appl. Energy*, vol. 98, pp. 479–490, Oct. 2012.
[31] Z. Y. Song, H. Hofmann, J. Q. Li, J. Hou, X. B. Han, and M. G. Ouyang, "Energy management strategies comparison for electric vehicles with hybrid energy storage system," *Appl. Energy*, vol. 134, pp. 321–331, Dec. 2014.
[32] B. Hredzak, V. G. Agelidis, and M. Jang, "A model predictive control system for a hybrid battery-ultracapacitor power source," *IEEE Trans. Power Electron.*, vol. 29, no. 3, pp. 1469–1479, Mar. 2014.
[33] S. Zhang, R. Xiong, and F. C. Sun, "Model predictive control for power management in a plug-in hybrid electric vehicle with a hybrid energy storage system," *Appl. Energy*, vol. 185, pp. 1654–1662, Jan. 2017.
[34] C. Sun, X. S. Hu, S. J. Moura, and F. C. Sun, "Velocity predictors for predictive energy management in hybrid electric vehicles," *IEEE Trans. Control Syst. Technol.*, vol. 23, no. 3, pp. 1197–1204, May 2015.
[35] E. Vinot and R. Trigui, "Optimal energy management of HEVs with hybrid storage system," *Energy Convers. Manag.*, vol. 76, pp. 437–452, Dec. 2013.
[36] H. Borhan, A. Vahidi, A. M. Phillips, M. L. Kuang, I. V. Kolmanovsky, and S. Di Cairano, "MPC-Based energy management of a power-split hybrid electric vehicle," *IEEE Trans. Control Syst. Technol.*, vol. 20, no. 3, pp. 593–603, May 2012.
[37] N. Kim, S. Cha, and H. Peng, "Optimal control of hybrid electric vehicles based on pontryagin's minimum principle," *IEEE Trans. Control Syst. Technol.*, vol. 19, no. 5, pp. 1279–1287, Sep. 2011.
[38] C. W. Zheng, Y. L. Ge, Z. Q. Chen, D. Y. Huang, J. Liu, and S. Y. Zhou, "Diagnosis method for Li-Ion battery fault based on an adaptive unscented kalman filter," *Energies*, vol. 10, no. 11, pp. 1–14, Nov. 2017.
[39] G. L. Plett, "Extended Kalman filtering for battery management systems of LiPB-based HEV battery packs-Part 2. Modeling and identification," *J. Power Sour.*, vol. 134, no. 2, pp. 262–276, Aug. 2004.
[40] C. Forgez, D. V. Do, G. Friedrich, M. Morcrette, and C. Delacourt, "Thermal modeling of a cylindrical LiFePO4/graphite lithium-ion battery," *J. Power Sour.*, vol. 195, no. 9, pp. 2961–2968, May 2010.
[41] R. Xiong, F. C. Sun, H. W. He, and T. D. Nguyen, "A data-driven adaptive state of charge and power capability joint estimator of lithium-ion polymer battery used in electric vehicles," *Energy*, vol. 63, pp. 295–308, Dec. 2013.
[42] H. W. He, X. W. Zhang, R. Xiong, Y. L. Xu, and H. Q. Guo, "Online model-based estimation of state-of-charge and open-circuit voltage of lithium-ion batteries in electric vehicles," *Energy*, vol. 39, no. 1, pp. 310–318, Mar. 2012.
[43] C. Chen, R. Xiong, and W. X. Shen, "A lithium-ion battery-in-the-loop approach to test and validate multiscale dual H infinity filters for state-of-charge and capacity estimation," *IEEE Trans. Power Electron.*, vol. 33, no. 1, pp. 332–342, Jan. 2018.
[44] K. Deb, S. Agrawal, A. Pratap, and T. Meyarivan, "A fast elitist non-dominated sorting genetic algorithm for multi-objective optimization: NSGA-II, in parallel problem solving from nature PPSN VI," in *Proc. 6th Int. Conf.*, 2000, pp. 849–858.

Shiyao Zhou received the M.S. degree from the Department of Naval Architecture, Ocean and Civil Engineering, Shanghai Jiao Tong University, Shanghai, China, in 2020. He is currently working toward the Ph.D. degree in major of marine engineering with the State Key Laboratory of Ocean Engineering, Shanghai Jiao Tong University, China.

His current research interests include the areas of the hybrid power system energy management and battery fault-tolerant state estimate.

Ziqiang Chen (Senior Member, IEEE) received the Ph.D. degree in mechanical engineering from Xian Jiaotong University, Xian, China, in 1999.

From 2011 to 2012, he worked as a Visiting Scholar with the Department of Electrical and Computer Engineering, Wayne State University, Detroit, MI, USA. Since 2007, he has been with Shanghai Jiao Tong University, Shanghai, China, where he is currently a Professor with the Department of Naval Architecture, Ocean and Civil Engineering. His research interests include the areas of system identification and state estimation, fault diagnosis, discrete-event systems, automotive and electric vehicle control, battery management systems, composite energy storage system, intelligent industrial detection, robot application, and intelligent manufacturing.

Dr. Chen was recipient of the National Scientific Conference Award, Ministerial Second Prize Award, and Excellence Award of Chinese Invention Patent.

Deyang Huang received the B.S. degree in marine engineering from Wuhan University of Technology, Wuhan, China, in 2016. He is currently working toward the Ph.D. degree in marine engineering with the State Key Laboratory of Ocean Engineering, Shanghai Jiao Tong University, Shanghai, China.

His current research interests include the design of battery thermal management system working at extremely cold temperatures and the application of state estimation algorithms in battery management system.

Tiantian Lin received the B.S. degree in naval architecture and marine engineering from Harbin Engineering University, Harbin, China, in 2017. She is currently working toward the Ph.D. degree in marine engineering with the State Key Laboratory of Ocean Engineering, Shanghai Jiao Tong University, Shanghai, China.

Her current research interests include fault diagnosis and fault-tolerant state estimate of batteries.